NASA/TP–2013-217965

Correlated Uncertainties in Radiation Shielding Effectiveness

Charles M. Werneth
Langley Research Center, Hampton, Virginia

Khin Maung Maung
University of Southern Mississippi, Hattiesburg, Mississippi

Steve R. Blattnig and Martha S. Clowdsley
Langley Research Center, Hampton, Virginia

Lawrence W. Townsend
University of Tennessee, Knoxville, Tennessee

February 2013

NASA STI Program . . . in Profile

Since its founding, NASA has been dedicated to the advancement of aeronautics and space science. The NASA scientific and technical information (STI) program plays a key part in helping NASA maintain this important role.

The NASA STI program operates under the auspices of the Agency Chief Information Officer. It collects, organizes, provides for archiving, and disseminates NASA's STI. The NASA STI program provides access to the NASA Aeronautics and Space Database and its public interface, the NASA Technical Report Server, thus providing one of the largest collections of aeronautical and space science STI in the world. Results are published in both non-NASA channels and by NASA in the NASA STI Report Series, which includes the following report types:

- TECHNICAL PUBLICATION. Reports of completed research or a major significant phase of research that present the results of NASA Programs and include extensive data or theoretical analysis. Includes compilations of significant scientific and technical data and information deemed to be of continuing reference value. NASA counterpart of peer-reviewed formal professional papers, but having less stringent limitations on manuscript length and extent of graphic presentations.

- TECHNICAL MEMORANDUM. Scientific and technical findings that are preliminary or of specialized interest, e.g., quick release reports, working papers, and bibliographies that contain minimal annotation. Does not contain extensive analysis.

- CONTRACTOR REPORT. Scientific and technical findings by NASA-sponsored contractors and grantees.

- CONFERENCE PUBLICATION. Collected papers from scientific and technical conferences, symposia, seminars, or other meetings sponsored or co-sponsored by NASA.

- SPECIAL PUBLICATION. Scientific, technical, or historical information from NASA programs, projects, and missions, often concerned with subjects having substantial public interest.

- TECHNICAL TRANSLATION. English-language translations of foreign scientific and technical material pertinent to NASA's mission.

Specialized services also include organizing and publishing research results, distributing specialized research announcements and feeds, providing information desk and personal search support, and enabling data exchange services.

For more information about the NASA STI program, see the following:

- Access the NASA STI program home page at *http://www.sti.nasa.gov*

- E-mail your question to help@sti.nasa.gov

- Fax your question to the NASA STI Information Desk at 443-757-5803

- Phone the NASA STI Information Desk at 443-757-5802

- Write to:
  STI Information Desk
  NASA Center for AeroSpace Information
  7115 Standard Drive
  Hanover, MD 21076-1320

NASA/TP–2013-217965

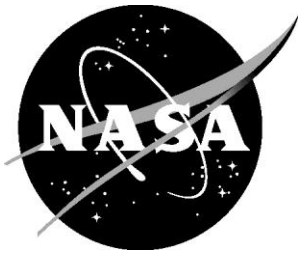

Correlated Uncertainties in Radiation Shielding Effectiveness

Charles M. Werneth,
Langley Research Center, Hampton, Virginia

Khin Maung Maung
University of Southern Mississippi, Hattiesburg, Mississippi

Steve R. Blattnig and Martha S. Clowdsley
Langley Research Center, Hampton, Virginia

Lawrence W. Townsend
University of Tennessee, Knoxville, Tennessee

National Aeronautics and
Space Administration

Langley Research Center
Hampton, Virginia 23681-2199

February 2013

Acknowledgments

The authors would like to thank Drs. Robert Singleterry and Francis Badavi for their useful suggestions during the course of this research. Furthermore, the authors would like to thank Drs. Tony Slaba, Ryan Norman, Francis Badavi, John Norbury, and Jonathan Ransom for reviewing this manuscript. This work was supported in part by NASA grants NNX10AD18A and NNX08AI53A.

Contents

Nomenclature

CI	Confidence Interval
DDREF	Dose and Dose Rate Reduction Factor
E	Kinetic energy per nucleon of particle
EAR	Excess Additive Risk
ED	Effective Dose
ERR	Excess Relative Risk
F(E)	Fluence
GCR	Galactic Cosmic Rays
ICRP	International Commission on Radiological Protection
IMF	Interplanetary Magnetic Field
LET	Linear Energy Transfer
m	Radiation cancer mortality rate
M	Mortality rate of background population
m_c	Cancer mortality rate of background population
m_l	Low LET mortality rate
NCRP	National Council on Radiation Protection and Measurements
PDF	Probability Distribution Function
PY	Person Year
Q	Quality factor

REID	Risk of exposure induced death
SEER	Surveillance, Epidemiology, and End Results
SPE	Solar Particle Event

List of Figures

List of Tables

Abstract

The space radiation environment is composed of energetic particles which can deliver harmful doses of radiation that may lead to acute radiation sickness, cancer, and even death for insufficiently shielded crew members. Spacecraft shielding must provide structural integrity and minimize the risk associated with radiation exposure. The risk of radiation exposure induced death (REID) is a measure of the risk of dying from cancer induced by radiation exposure. Uncertainties in the risk projection model, quality factor, and spectral fluence are folded into the calculation of the REID by sampling from probability distribution functions. Consequently, determining optimal shielding materials that reduce the REID in a statistically significant manner has been found to be difficult. In this work, the difference of the REID distributions for different materials is used to study the effect of composition on shielding effectiveness. It is shown that the use of correlated uncertainties allows for the determination of statistically significant differences between materials despite the large uncertainties in the quality factor. This is in contrast to previous methods where uncertainties have been generally treated as uncorrelated. It is concluded that the use of correlated quality factor uncertainties greatly reduces the uncertainty in the assessment of shielding effectiveness for the mitigation of radiation exposure.

1 Introduction

The space radiation environment consists of energetic particles which can deliver larger radiation doses than those experienced on Earth [1]. The assessment of risk from the space radiation environment is an important factor in the design and composition of spacecraft shielding, since materials must be chosen that maintain structural integrity and provide optimum mitigation of radiation for crew members and instrumentation. Failure to properly shield instrumentation could compromise the mission and endanger the life of astronauts. Moreover, the effect of radiation on astronauts could lead to acute radiation sickness, cancer, or even death if crew members are insufficiently shielded. It is from these consequences that the following question arises: Which shielding materials and thicknesses provide optimum radiation mitigation for crew members? Before this question can be answered, a measure of risk associated with radiation exposure must be defined.

Although many measures of risk exist, NASA uses a career radiation exposure limit [2] of 3% REID [3, 4, 5, 6, 7, 8], which is based on models of radiation cancer mortality rates and background mortality data. The life span study (LSS) of the Japanese Hiroshima atomic bomb cohort is a major source of radiation cancer mortality data [9, 10, 11]. In

this ongoing study, the number of cancer deaths of a cohort located within 3 km of the atomic bomb hypocenter is monitored. A control group of similar size and composition is also monitored within 3-10 km of the atomic bomb hypocenter, where radiation exposure was assumed to be negligible. Radiation cancer mortality models are based on comparisons of the exposed cohort to the control group. There are several uncertainties that must be incorporated into the REID when using risk models developed from the LSS. These uncertainties include the extrapolation of the relatively high doses received by the Japanese Hiroshima atomic bomb cohort to low radiation doses, the reported number of cancer related deaths, measurements of dosimetry, and the transfer of risk from the Japanese to other populations [8]. In this document, the aforementioned uncertainties are collectively referred to as uncertainties in the low linear energy transfer (LET) risk projection model, where LET is the energy lost by a particle per unit path length into a material.

The effective dose is also needed for evaluation of the REID and depends on the quality factor [12], particle fluence, and LET. The quality factor is the largest source of uncertainty in the estimation of risk for the space radiation environment [3, 13] and is derived from the maximum relative biological effectiveness (RBE), which is obtained from experiments on animals and human tissue. The uncertainty in the quality factor is largely due to insufficient experimental data for various sources of ionizing radiation and energy ranges relevant to the space radiation environment. In addition to quality factor uncertainties, there is also a degree of uncertainty associated with the spectral fluence. Estimates of the spectral fluence uncertainties are obtained from comparisons of radiation transport codes to space dosimetry measurements [3, 13, 14].

The quality factor, fluence, and low-LET uncertainties have been incorporated into the calculation of the probabilistic effective dose and the REID by Cucinotta et al. [3]. In that work, a χ^2 analysis was used to show that differences in shielding effectiveness among materials were not statistically significant, but it was assumed that the quality factor and fluence uncertainties were uncorrelated, or had no interdependence. However, the quality factor and low-LET uncertainties described in [3], and in the current document, depend only on LET; there is no dependence of material composition. In the current document, the use of correlated uncertainties is shown to greatly reduce the overall uncertainty in the difference of distributions and allows for the identification of materials which reduce the overall risk for most of the cases studied herein.

This document is organized as follows. In section 2, the REID is derived from the cause specific risk of death. Other measures of risk, such as the lifetime attributable risk (LAR) and estimated lifetime risk (ELR), are also described. In sections 2.1 and 2.2, the space radiation environment, radiation transport, and the effective dose are discussed. This is followed by a discussion of the quality factor and the radiation cancer mortality rate in sections 2.3 and 2.4. In section 3, the quality factor, fluence (physics), and low-LET uncertainties are described. Note that the description given in this section closely follows the discussion of Cucinotta et al. [3]. In the current work, the functional forms

of probability distributions are explicitly stated. Furthermore, some of the distributions in this work differ from those used by Cucinotta et al. [3]; thus, for the sake of clarity, all distributions were described. In section 4, the uncertainties described in section 3 are incorporated into the effective dose and the REID. Section 5 includes a discussion of the latency model used for solid cancer and leukemia.

The work presented in sections 2-5 is not original research. Much of this work has been documented in Cucinotta et. al [3]. It has been presented in this document so that the results that follow can be unequivocally reproduced. The distributions used for the projection of the fluence uncertainty and the maximum quality factor differ slightly from those discussed in reference [3]. In addition, the distribution functions used in the current document have been stated explicitly.

Calculations of the non-probabilistic and probabilistic effective dose and the REID are verified in section 6. In section 7, material analysis is performed with the percent difference of the effective dose and the REID distributions for different materials. The effect of using correlated uncertainties is shown to reduce the overall uncertainty in the difference of distributions thus allowing for the better identification of materials and shielding strategies. The conclusions are stated in section 8.

2 Risk

In this section, the REID and other measures of risk are described. First, the cause specific risk of death is written as a function of the cause specific mortality rate and the probability of survival of the background population. The background survival probabilities are calculated from the probability of death using mortality data. Next, the REID is written as a variation of the cause specific risk of death in which the cause specific mortality rate is expressed as a function of the radiation cancer mortality rate, and the probability of survival becomes a function of effective dose. The radiation cancer mortality rate depends on the cancer mortality rate of the background population and models of radiation induced cancer deaths. The exposed probability of survival becomes a function of effective dose and radiation cancer mortality rates.

Mortality data are usually listed in the form of life tables. The background mortality rate for all causes of death is taken from the National Vital Statistics Reports (NVSR) [15]. Cancer specific mortality rates are taken from Surveillance Epidemiology and End Results (SEER) [16]. The primary source of data for radiation induced cancer deaths comes from the Japanese Hiroshima cohort, where radiation cancer mortality rates have been modeled [9, 10, 11]. A full discussion of the background mortality rates and cancer specific mortality is found in Appendix A.

The cause specific risk of death is defined by the following integral [6]:

$$R_\gamma \equiv \int_\alpha^\beta m_\gamma(a)\tilde{S}(a|\alpha)da, \tag{1}$$

where a is the age; α and β are the initial and final ages, respectively; $m_\gamma(a)$ is the mortality rate for cause γ; and $\tilde{S}(a|\alpha)$ is the conditional probability of survival for the background population, which is given by [6],

$$\tilde{S}(a|\alpha) = \frac{S(a)}{S(\alpha)}, \tag{2}$$

where $S(a)$ is the probability of survival. In practice, the integral can be approximated by summing over one year intervals:

$$R_\gamma = \int_\alpha^\beta m_\gamma(a)\tilde{S}(a|\alpha)da \approx \sum_{a=\alpha}^{\beta} m_\gamma(a)\tilde{S}(a|\alpha). \tag{3}$$

The definition of the mortality rate for cause γ is given by [17]

$$m_\gamma(a) = \frac{\text{number of deaths from cause } \gamma}{\text{number of person years lived}}. \tag{4}$$

A person year (PY) is the total number of people exposed to radiation multiplied by the average number of years in which the cohort was studied after the radiation exposure [8].

There is an important difference between the definition of mortality rate and probability of death. The denominator in the definition of the probability of death is the number of people years *lived* during a given time interval. One must account for the number of people who lived through the entire age interval and the total number of years lived by those who died before the end of the interval. On average, the number of deaths occurring during a given time interval is evenly distributed across that time interval, but there are exceptions. For example, infant deaths usually occur during the first few weeks after birth. The number of years lived by those who die in a given interval is given by the number of deaths times the ratio factor, a_x, that describes the distribution of lives to deaths on the interval. For N_D number of deaths of cause γ and N_{PY} number of people years, the probability of death in the age interval $[a_i, a_{i+1}]$ is given by [15, 17]

$$q_\gamma = \frac{N_D}{N_{PY} + a_x N_D}. \tag{5}$$

Dividing the numerator and denominator by the number of people years N_{PY} in the

interval results in [15, 17]

$$q_\gamma(a) = \frac{m_\gamma(a)}{1 + a_x m_\gamma(a)}. \tag{6}$$

If the ratio of lives to deaths is assumed to be evenly distributed across the interval for all ages, then $a_x = 1/2$ and [15, 17]

$$q_\gamma(a) = \frac{m_\gamma}{1 + \frac{1}{2} m_\gamma}, \tag{7}$$

where the time interval is taken to be one year. The probability of survival is calculated from the probability of death and is given by the following product [3]:

$$S(a) = \prod_{u=a_i}^{a} [1 - q_\gamma(u)], \tag{8}$$

where a_i is some initial age of interest and a is the attained age.

To calculate the REID, the exposed probability of survival and the radiation cancer mortality rate are needed. The REID is given by using an altered form of equation 3, where the lower limit occurs at the age of radiation exposure a_E, and the upper limit is the maximum attained age possible, which is taken to be $a_{max} \approx 101$ yr [3]. The REID is given by [3, 5]

$$\text{REID} = \sum_{a=a_E}^{a_{max}} m(a, a_E, ED) \hat{S}(a, ED|a_E), \tag{9}$$

where $m(a, a_E, ED)$ is the radiation cancer mortality, a is the age, a_E is the age of exposure, ED is the effective dose, and $\hat{S}(a, ED|a_E)$ is the conditional exposed probability of survival given by [6],

$$\hat{S}(a, ED|a_E) = S(a, ED)/S(a_E, ED). \tag{10}$$

The conditional exposed probability of survival is calculated from the probability of death, q, in the interval $[a_i, a_{i+1}]$ for a given radiation dose. In order to compute the probability of death, m_γ in equation (7) is replaced with $m_\gamma \equiv M(a) + m(a, a_E, ED)$, where $M(a)$ is the background US mortality rate for all causes of death. Therefore, equation (7) becomes [3, 17]

$$q(a, a_E, ED) = \frac{M(a) + m(a, a_E, ED)}{1 + \frac{1}{2}[M(a) + m(a, a_E, ED)]}. \tag{11}$$

As in equation (8), the probability of survival for a given radiation dose is expressed as

[3]

$$\hat{S}(a, ED) = \prod_{u=a_E}^{a_{\max}} [1 - q(u, a_E, ED)]. \tag{12}$$

The present work focuses on calculation of the REID; however, there are other ways to quantify risk. The lifetime attributable risk (LAR) is defined as [3, 4]

$$\begin{aligned} \text{LAR} \equiv & \int_{a_E}^{a_{max}} m(a, a_E, ED)\tilde{S}(a|a_E)da \\ & \approx \sum_{a=a_E}^{a_{max}} m(a, a_E, ED)S(a)/S(a_E), \end{aligned} \tag{13}$$

where a is the age, a_E is the age of exposure, $m(a)$ is the radiation cancer mortality rate, and $\tilde{S}(a|a_E)$ is the conditional probability of survival for the background population described by equation (8). Note that the above probability of survival for the LAR is independent of effective dose.

Another risk quantity used frequently is the estimated lifetime risk (ELR), the excess risk that a person will die from radiation induced cancer as compared to the background cancer population [3], and is defined as [5]

$$\begin{aligned} \text{ELR} \equiv & \sum_{a=a_E}^{a_{max}} [m(a, a_E, ED) + m_c(a)]\hat{S}(a, ED|a_E) \\ & - \sum_{a=a_E}^{a_{max}} m_c(a)\tilde{S}(a|a_E), \end{aligned} \tag{14}$$

where $m(a, a_E, ED)$ is the radiation cancer mortality rate, and $m_c(a)$ is the cancer mortality rate of the background population. $\hat{S}$ is the exposed probability of survival and $\tilde{S}$ is the background probability of survival. The trends of the LAR, ELR, and the REID as a function of effective dose are used to verify the results in the present work.

The effective dose and the radiation cancer mortality rate are needed to calculate the REID. In the next section, the space radiation environment and effective dose are described. This is followed by a discussion of the quality factor and models of the radiation cancer mortality rate.

2.1 Space Radiation Environment

The space radiation environment consists of particles that are trapped in Earth's radiation belts (ERBs), solar particle events (SPEs), and galactic cosmic rays (GCRs) [1]. Earth is surrounded by energetic protons and electrons that have become trapped in the

geomagnetic field, known as the Van Allen radiation belts. In ERBs, proton energies can reach hundreds of MeV, and electrons energies extend up to hundreds of keV and higher. SPEs are primarily composed of protons generated from solar flares and coronal mass ejections. These events are relatively rare and usually last from a few hours up to a couple of days and can deliver a potentially lethal dose of radiation to unshielded crew members. The proton energies in these events can reach up to several GeV. GCRs consist of protons and heavier ions with energies reaching up to several GeV per nucleon. The shock waves of supernovae are believed to be the source of GCRs [1, 18]. Due to the uniform distribution of supernovae throughout the galaxy, the GCR flux of particles that stream into the solar system is fairly constant.

The interplanetary magnetic field (IMF) generated by the sun modulates the intensity of GCR particle flux [18]. The IMF is dependent on the solar cycle, which varies over a period of 11 years between maxima. During solar maximum, the GCR particle flux is attenuated the greatest; whereas, at solar minimum, the GCR particle flux is attenuated the least. In the next section, the interaction of particles with the vehicle and the effective dose are described.

2.2 Particle Transport and Effective Dose

As particles from the space radiation environment encounter spacecraft, elastic scattering, inelastic scattering and, reactions (fragmentation) may occur [19]. Elastic collisions describe the scattering of two particles when there is no change in the internal structure of the projectile and target after the collision. Inelastic collisions refer to scattering that results in changes of the internal structure of the particles after the collision. Finally, reactions (fragmentation) refer to the break-up of the projectile and (or) the target into particles that are different from the initial projectile and (or) target.

Radiation transport is the process in which incident particles from the space radiation environment, and any particles that result from their subsequent collisions with nuclei in the shield, propagate through the shield and into the body. This process may be described with the Boltzmann transport equation. It is difficult to solve the Boltzmann equation for complex three-dimensional vehicle geometries. As a result, NASA developed the deterministic transport code, High charge (Z) and Energy TRaNsport (HZETRN) [20, 21, 22]. To simplify the radiation transport, the assumption is made that particles moving in one direction before an interaction continue to move in the same direction after the interaction. This is known as the straight ahead approximation, and it reduces the complex three-dimensional vehicle calculations to a series of one-dimensional transport solutions which can be integrated.

Once the particles have penetrated the shield, astronauts and instrumentation will then be exposed to the radiation. The effects of the radiation on the human body are studied in order to estimate radiation risks. The dose, dose equivalent, and effective dose equivalent are used extensively for radiation risk. The dose at a point is the energy

absorbed per unit mass and is given by

$$D = \sum_k \int_0^\infty \Phi_k(E) S_k(E) dE, \tag{15}$$

where k is the summation index for each ion, E is the kinetic energy per nucleon for a given particle, $\Phi_k(E)$ is the energy dependent particle flux, and $S_k(E)$ is the particle specific stopping power. For an infinite-sized medium, the stopping power can be replaced with the linear energy transfer (LET), the energy absorbed per unit length in a material. Note that lengths are often expressed in units of areal density g/cm^2, which is obtained by multiplying the length [cm] by the density [g/cm^3].

The effect of radiation on biology is needed for determining radiation risk. The dose equivalent is similar to the dose except the quality factor is folded into the integral to take into account the biological effect of the radiation. The dose equivalent at a point is defined as

$$H \equiv \sum_k \int_0^\infty \Phi_k(E) L_k(E) Q(L_k(E)) dE \tag{16}$$

where Q is the quality factor as of function of the LET in the energy domain.

The effective dose is used as a measure of the effect of radiation on the body. The damage incurred from radiation exposure varies among the organs in the body. Tissue weighting factors are used to account for these differences in calculations. The following computation procedure is used with HZETRN to compute effective dose. Each organ is represented by a set of (approximately) equally spaced points. Rays representing the path of radiation are traced from the outermost shield to a point in the organ. The dose equivalent is obtained for each of the points located in the organ. The organ dose equivalent is calculated by averaging over the dose equivalents at each point in the organ. The effective dose is the weighted sum of the organ dose equivalents and is given as [13]

$$\mathrm{ED} = \sum_k \sum_i \frac{w_i}{m_i} \int_0^{m_i} dm_i \int_0^\infty \Phi_k(E) L_k(E) Q(L_k(E)) dE, \tag{17}$$

where dm_i is the differential mass element of each organ i, w_i are the tissue weighting factors, and m_i are the total organ masses. In addition, an effective flux $F_k(E)$ may be defined as

$$F_k(E) \equiv \sum_i \frac{w_i}{m_i} \int_0^{m_i} dm_i \Phi_k(E) \tag{18}$$

such that the effective dose becomes [3]

$$\mathrm{ED} = \sum_k \int_0^\infty F_k(E) L_k(E) Q(L_k(E)) dE. \tag{19}$$

The effective dose is a function of the flux, LET, and the quality factor. The effective dose is used to the calculate the REID, an important indicator of the risk associated with space radiation. Before calculating the effective dose, the quality factor must be defined. This description is given in the following section.

2.3 Quality Factor

In the last section, the dose was defined as the amount of energy deposited in a material per unit mass. A definition that takes into account the biological effect of the radiation on different tissues is needed. The relative biological effectiveness (RBE) was first introduced to take into account the absorbed dose and biological effect of radiation [23]. The RBE was defined as the absorbed dose from gamma rays or x-rays that produce a certain biological effect divided by the the absorbed dose from some other source of radiation that produces the same biological effect. There are some problems with this definition. The RBE is not unique because it depends on the radiation energy, the biological target, and many other factors [23]. The International Commission on Radiological Units of Measurements (ICRU) defined a factor that modifies the absorbed dose for all types of ionizing radiation. This factor is known as the quality factor Q and is defined as function of linear energy transfer (LET) in water, which has been chosen because of the large composition of water in the human body. The ICRP-60 [12] definition of the quality factor is given by

$$Q_{60}(L) = \begin{cases} 1 & \text{for } L \leq 10\,\mathrm{keV}/\mu\mathrm{m} \\ 0.32\,L - 2.2 & \text{for } 10\,\mathrm{keV}/\mu\mathrm{m} \leq \mathrm{L} \leq 100\,\mathrm{keV}/\mu\mathrm{m} \\ \frac{300}{L^{0.5}} & \text{for } L \geq 100\,\mathrm{keV}/\mu\mathrm{m} \end{cases} \tag{20}$$

where L is the LET.

The quality factor and effective dose are both needed for the calculation of the REID and have been described. The final component of the REID calculation is the radiation cancer mortality rate. This is discussed in the next section.

2.4 Radiation Cancer Mortality Rate

The LSS of the Hiroshima atomic bomb cohort is the major source of radiation cancer mortality data [9, 10, 11]. In this ongoing study, the age and gender specific cancer mortality rates of a cohort located within 3 km of the atomic blast hypocenter are monitored.

A control group of similar size, sex, and age composition is studied from 3 -10 km outside of the hypocenter, where radiation doses from the atomic blast is assumed to be negligible. Radiation cancer models are based on comparisons of the cancer mortality rates of the group located within 3 km of the hypocenter to the control group.

The radiation risk is modeled by the excess absolute risk (EAR) and excess relative risk (ERR). The EAR is the absolute difference of the mortality between those who are exposed to given dose of radiation and those who are unexposed for a given age and sex [24]. The ERR is defined in terms of the observed number of cancer deaths O and the expected number of cancer deaths E [8]:

$$ERR = \frac{O - E}{E}. \tag{21}$$

The radiation cancer mortality data for the LSS cohort consist of solid cancers and leukemia. The general trend of EAR and ERR is different for solid cancer and leukemia, and two different models will be used. The radiation cancer mortality rate is given by [3]

$$m = m_0^S \chi_\alpha^S + m_0^L \chi_\alpha^L, \tag{22}$$

where m_0 is baseline mortality rate, χ_α are statistical factors related to the low LET uncertainties described in the following section, and S and L represent solid cancer and leukemia, respectively. In general, the baseline mortality rate may be modeled as a function of the ERR, EAR, and the cancer mortality rate $m_c(a)$ [3]:

$$\begin{aligned} m_0 = \eta ERR(a, a_E, ED) m_c(a) \\ + (1 - \eta) EAR(a, a_E, ED), \end{aligned} \tag{23}$$

where a is the age, a_E is the age of exposure, ED is the effective dose, $\eta = 0$ for leukemia and $\eta = 0.5$ for solid cancer [3]. The solid cancer models for EAR and ERR use a linear dose response, whereas the leukemia models are based on a linear-quadratic effective dose response [9, 10, 11]. For leukemia, either an EAR or ERR model is used. In this paper, the EAR model has been used [9].

2.4.1 Solid Cancer

Solid cancer is defined as all malignant neoplasms, excluding cancers of the blood [25], and examples include cancers of the heart, liver, breast, and prostate. The solid cancer baseline mortality rate is given as [3]

$$\begin{aligned} m_0^S = 0.5 ERR(a, a_E, ED) m_c^S(a) \\ + 0.5 EAR(a, a_E, ED), \end{aligned} \tag{24}$$

where a is the age, a_E is the age of exposure, ED is the effective dose, and $m_c^S(a)$ is the solid cancer mortality rate. Preston et al. [11] model the sex averaged excess relative risk with the following:

$$\mathrm{ERR}_0 = 0.47 f(ED) \exp[-0.038(a_E - 30) - 0.70 \ln(\mathrm{a}/70)], \tag{25}$$

where the coefficient has units of Sv^{-1} and $f(ED) = ED$ is the linear dose response, which carries units of Sv. The ERR for males is 25 percent lower than ERR_0, and the ERR for females is 25 percent higher than ERR_0. For males, the ERR is

$$\mathrm{ERR} = \mathrm{ERR}_0 - 0.25\mathrm{ERR}_0, \tag{26}$$

and for females, the ERR is

$$\mathrm{ERR} = \mathrm{ERR}_0 + 0.25\mathrm{ERR}_0. \tag{27}$$

The solid cancer EAR per 10,000 PY is modeled by [11] as

$$\mathrm{EAR} = 30 f(ED) \exp[-0.027(a_E - 30) + 3.7 \ln(\frac{a}{70})], \tag{28}$$

where the coefficient has units of Sv^{-1} and $f(ED) = ED$ is the linear dose response with units of Sv. In the current work, the REID is calculated by summing over one-year intervals of the age in equation (9).

2.4.2 Leukemia

Leukemia is a malignant cancer of blood forming tissues, such as bone marrow or lymph nodes, and is characterized by excessive production of white blood cells [26]. The baseline mortality rate for leukemia can be expressed as a sole function of excess absolute risk [3, 9], with $\eta = 0$ in equation (24),

$$m_0^L = EAR. \tag{29}$$

The EAR model may be expressed as [9]

$$\mathrm{EAR} = g(ED) \exp[\beta_e + \gamma + (\delta_e + \epsilon) \ln(a/25)], \tag{30}$$

where $g(ED)$ is computed with a linear-quadratic model of the dose response

$$g(\mathrm{ED}) = \mathrm{ED} + \theta \mathrm{ED}^2, \tag{31}$$

where $\theta = 1.53$ Sv^{-1} for both sexes. For males, $\gamma = 0$ and $\epsilon = 0$, and for females, $\gamma = -0.335$ and $\epsilon = 0.483$. The coefficient of equation (30) is 1 Sv^{-1}. The remaining

parameters in equation (30) depend on the age of exposure and are summarized in Table 1 [9].

Table 1: Age at exposure dependent parameters for EAR [9].

	Ages 0-19	Ages 20-39	Ages 40+
β_e	-0.553	-0.037	0.708
δ_e	-1.542	-0.688	0.173

3 Uncertainties

In this section, uncertainties in the quality factor, the low LET risk projection, and the fluence (physics) are discussed. Quality factor uncertainties are guided by radiobiological experiments on animals and human tissue. Low LET risk model uncertainties represent the uncertainty in extrapolating risk models of the Japanese Hiroshima atomic bomb cohort to lower doses. Fluence uncertainties are estimated from comparisons of space radiation transport codes to space flight data [3, 14]. The authors of the current work use a fluence uncertainty of $\pm 15\%$ as described by Cucinotta et. al [3], although it should be noted that the uncertainty in fluence is not precisely known.

3.1 Uncertainty in Quality Factor

The quality factor is based on the maximum RBE obtained from biological studies of protons and heavier ions in animal tissue [3]. The uncertainty of the quality factor is the largest source of space radiation uncertainty due to the various sources and energies of ionizing radiation and sparseness of data in much of LET region of interest [3, 13].

The quality factor is defined as [3]

$$Q(L) = \begin{cases} 1 & \text{for } L \leq L_0 \\ AL - B & \text{for } L_0 \leq L \leq L_m \\ \frac{C}{L^p} & \text{for } L \geq L_m \end{cases} \tag{32}$$

where

$$A = \frac{Q_m - 1}{L_m - L_0} \quad \text{and} \quad B = \frac{Q_m L_0 - L_m}{L_m - L_0} \tag{33}$$

and

$$C = L_m^p Q_m. \tag{34}$$

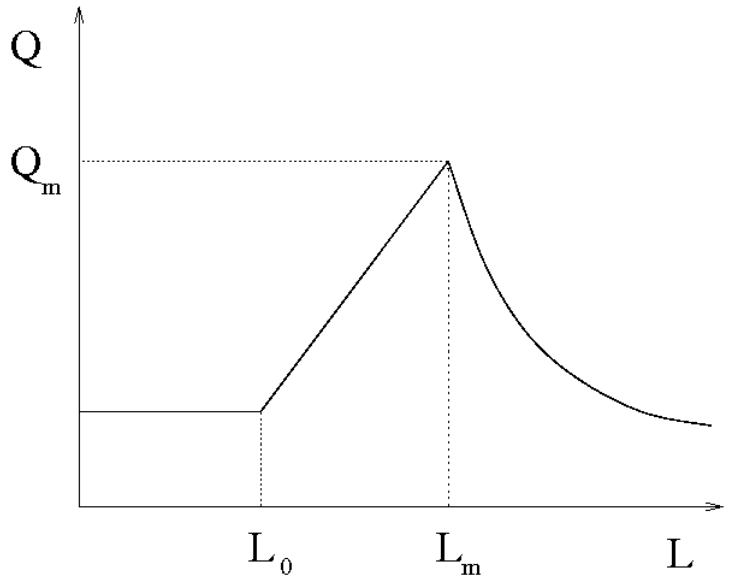

Figure 1: The quality factor

where L_0, L_m, Q_m, and p are sampled from probability distribution functions (PDFs) described below. The quality factor function is shown in Figure 1. After sampling from each distribution function, a unique quality factor can be constructed.

A description of the PDFs follows. A similar description is given by Cucinotta et al. [3]; however, there is no discussion on how the PDFs decrease to zero and increase from zero at the endpoints. The authors of the current work assume the functional forms of the PDFs increase from zero and decrease to zero linearly. Furthermore, a slightly larger geometric standard deviation was used for the Q_m distribution. Note that normalizations are arbitrary in the description that follows, as only relative PDFs are required for sampling deviates. (See Appendix B.)

- The Q_m PDF is a log-normal distribution with median of $e^{\mu} = 30$ [3, 24] and geometric standard deviation of $e^{\sigma} = 2.05$. The log-normal distribution is given as

$$P(x) = \frac{1}{\sqrt{2\pi\sigma^2}} \frac{1}{x} \exp\left[-\frac{(\log(x) - \mu)^2}{2\sigma^2}\right], \tag{35}$$

  where σ is the standard deviation and μ is the mean.

- The L_0 PDF is constant (set equal to 1) between 5 and 10 keV/μm [3, 24]. The distribution is assumed to increase linearly from 0 to 1 between 1 and 5 keV/μm

and decreases linearly from 1 to 0 between 10 to 15 keV/μm:

$$P(x) = \begin{cases} \frac{1}{4}x - \frac{1}{4} & \text{for } 1 \leq x \leq 5 \\ 1 & \text{for } 5 < x < 10 \\ -\frac{1}{5}x + 3 & \text{for } 10 \leq x \leq 15 \\ 0 & \text{elsewhere} \end{cases} \tag{36}$$

- The p PDF is constant (set equal to 1) between 1/2 and 1 [3, 24]. The distribution increases linearly from 0 to 1 between 0 and 1/2 keV/μm and decreases linearly from 1 to 0 from 1 to 2 keV/μm:

$$P(x) = \begin{cases} 2x & \text{for } 0 \leq x \leq \frac{1}{2} \\ 1 & \text{for } \frac{1}{2} < x < 1 \\ 2 - x & \text{for } 1 \leq x \leq 2 \\ 0 & \text{elsewhere} \end{cases} \tag{37}$$

- The L_m PDF is constant (set equal to 1) between 75 and 150 keV/μm [3, 24]. The distribution increases linearly from 0 to 1 between 50 to 75 keV/μm and decreases linearly from 1 to 0 between 150 and 250 keV/μm:

$$P(x) = \begin{cases} \frac{1}{25}x - 2 & \text{for } 50 \leq x \leq 75 \\ 1 & \text{for } 75 < x < 150 \\ -\frac{1}{100}x + \frac{5}{2} & \text{for } 150 \leq x \leq 250 \\ 0 & \text{elsewhere.} \end{cases} \tag{38}$$

The probability distribution functions obtained from 20,000 Monte Carlo samples are included in Figures 2-5. Deviates corresponding to the L_0, L_m, p, and Q_m distribution functions will be used to obtain the quality factor. Before proceeding to the discussion, the concept of a deviate should be defined. A deviate (or quantile) is a randomly sampled variable. Suppose there exists a distribution function $\rho(x)$. Randomly sampled x-values of the $\rho(x)$ distribution function are known as x-deviates. Likewise, random samplings of y-values of the $\rho(x)$ distribution are known as y-deviates. A full discussion of Monte Carlo sampling techniques is found in Appendix B.

Next, 20,000 Monte Carlo samples are accumulated and the 95% confidence intervals (Appendix C) for the quality factor are obtained using a set of LET values that ranges from 1 to 1000 keV/μm. The results of this calculation are found in Figure 6. This figure shows that there is great uncertainty for a large range of LET values, which is consistent with the results presented in reference [3]. The ICRP 60 definition of the quality factor

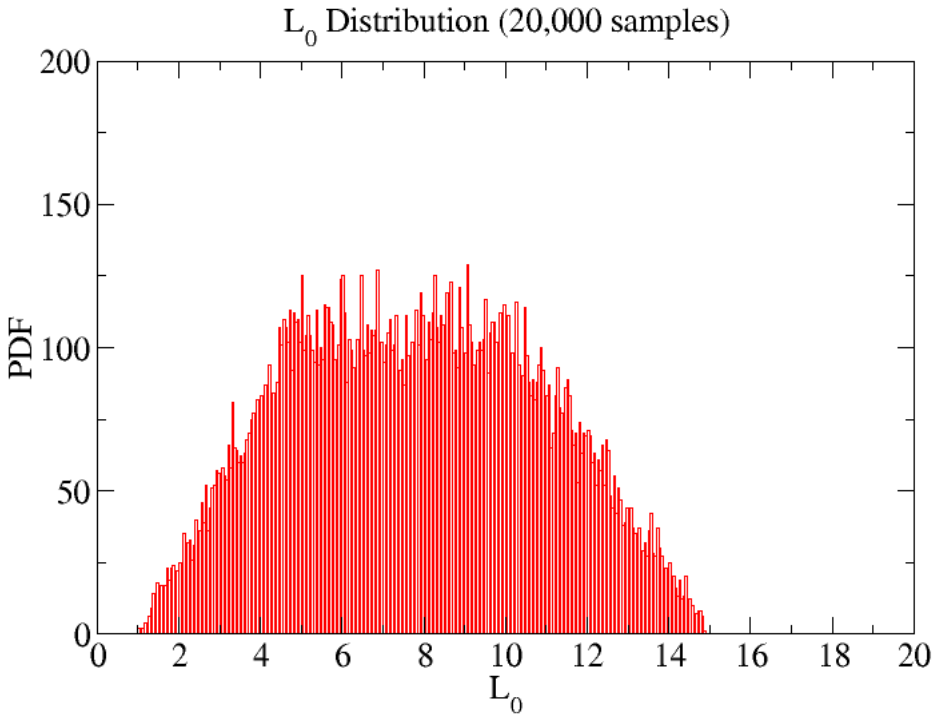

Figure 2: An example of the L_0 Probability Distribution Function using 20,000 samples.

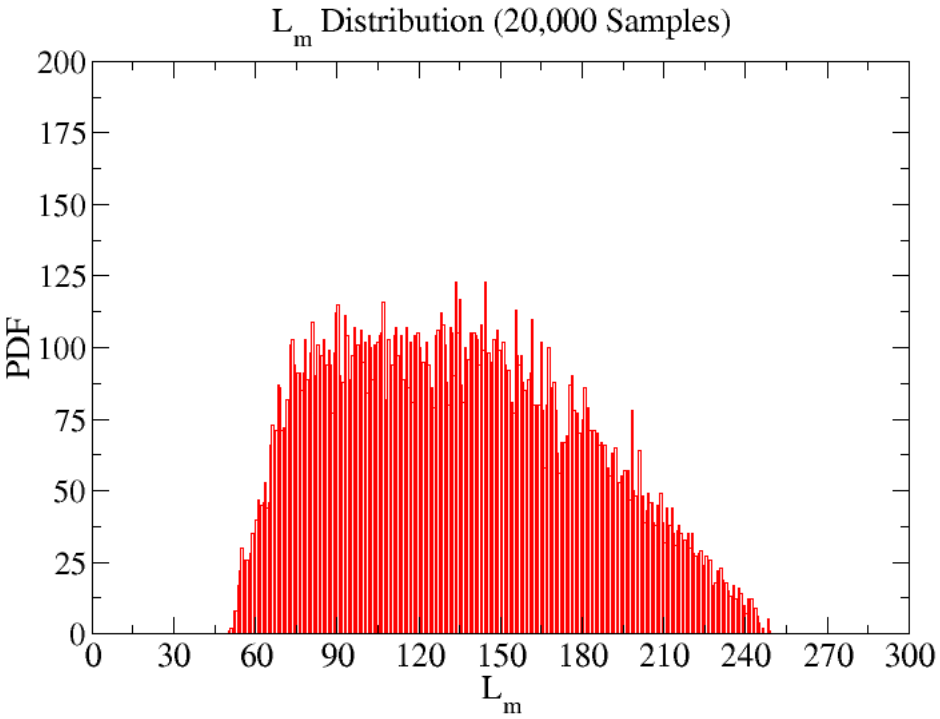

Figure 3: An example of the L_m Probability Distribution Function using 20,000 samples.

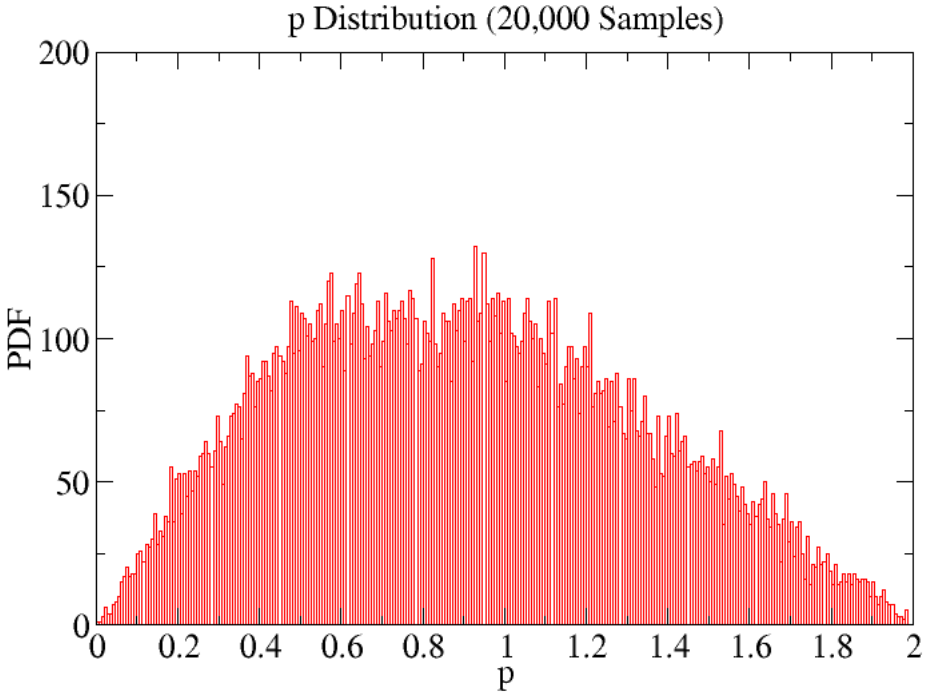

Figure 4: An example of the p Probability Distribution Function using 20,000 samples.

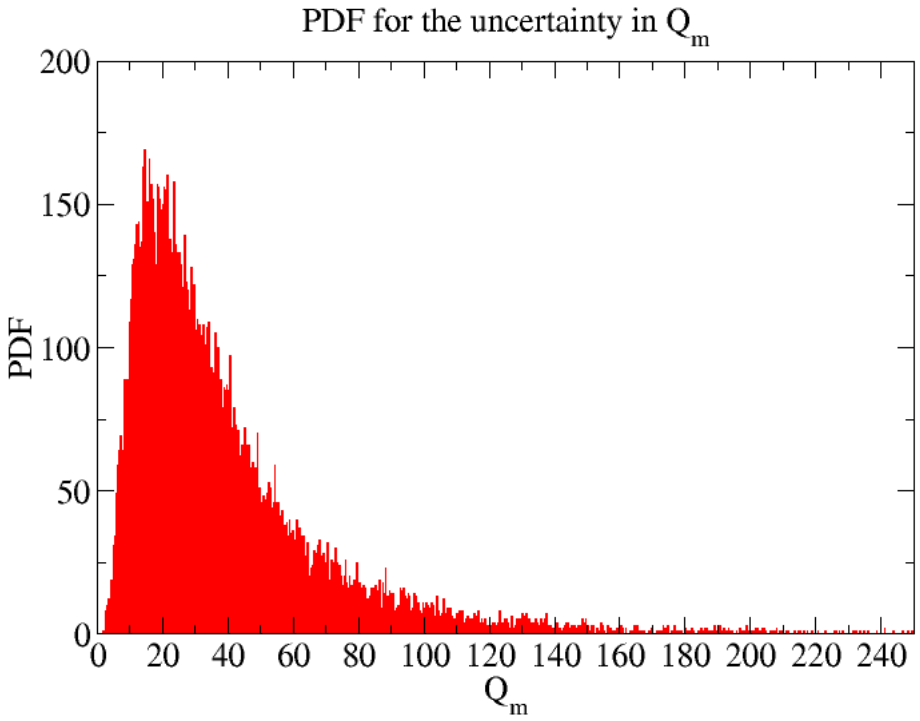

Figure 5: An example of the Q_m Probability Distribution Function using 20,000 samples.

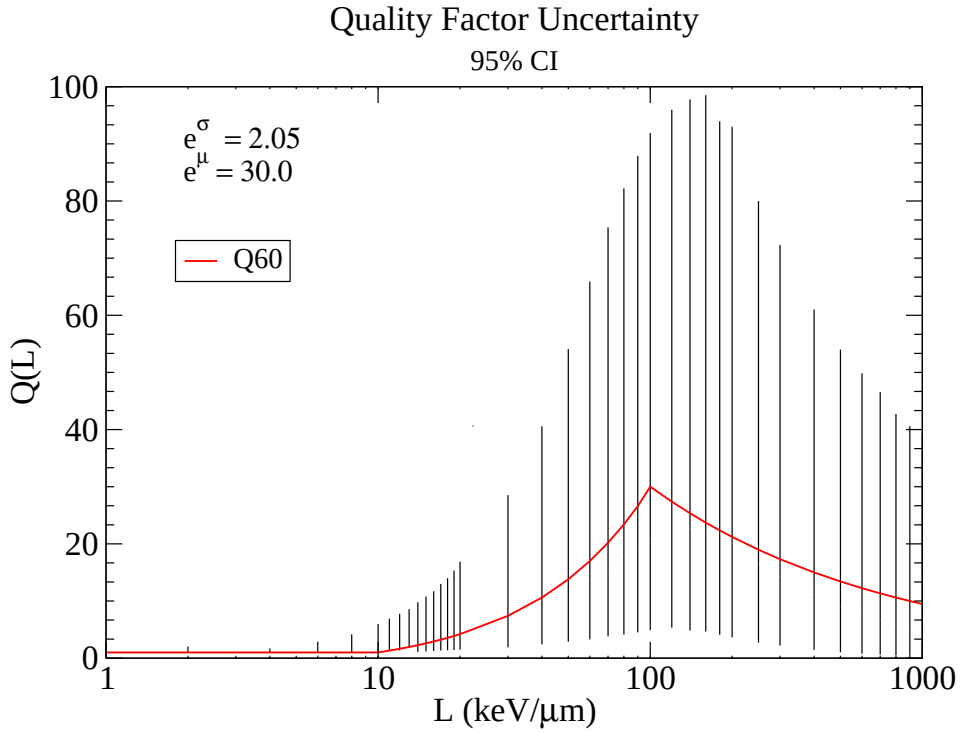

Figure 6: The 95% confidence interval for the LET dependent quality factor. 20,000 Monte Carlo samples were accumulated for each LET value. This figure indicates the large uncertainty in the quality factor for a broad range of LET values. The ICRP 60 definition of the quality factor is indicated by the red line. These results are consistent with those obtained in reference [3].

is indicated in red.

3.2 Uncertainty in Low LET Risk Model

NCRP 126 addresses uncertainties of fatal cancer induced by low-LET radiation [8]. The cancer mortality models described in section 2.4 of the current document are based on the Japanese atomic bomb cohort [9, 10, 11]. In this section, the uncertainties associated with extrapolating the atomic bomb risk models to lower doses is described. The low absorbed dose range is defined as 0 to 0.2 Gy; whereas, the low equivalent dose range is 0 to 0.2 Sv [8]. The low-LET uncertainty depends on deviates sampled from the PDFs described below. This description has also been given in Cucinotta et al. [3] and NCRP 126 [8]. It is restated here with an explicit functional form of the dose and dose rate reduction factor (DDREF) PDF, which follows from the discussion given in reference [8].

- P_{DDREF} is the PDF associated with the uncertainty in the DDREF, which is defined by NCRP 126 to be the linear term of the linear-quadratic dose response model [8]. At low dose and dose rates, the slope of a linear dose response model is reduced by dividing by the DDREF. A truncated triangle distribution is used for the uncertainty in DDREF. The most probable value is 2, but the uncertainty is expressed as a factor of 2 to 2.5 from the most probable value. A DDREF of 1 is 1/4 as likely as a DDREF of 2, and a DDREF of 3 is 1/2 as likely as a DDREF of 2. In addition, the DDREF PDF decreases linearly from a DDREF of 3 to 5. The distribution has a most probable value of 2 with a 90% CI of 1.25 to 4.13 and is given by

$$P(x) = \begin{cases} \left(\frac{3}{4}x - \frac{1}{2}\right) & \text{for } 1 \leq x \leq 2 \\ \left(\frac{-1}{2}x + 2\right) & \text{for } 2 < x \leq 3 \\ \left(\frac{-1}{4}x + \frac{5}{4}\right) & \text{for } 3 < x \leq 5 \\ 0 & \text{elsewhere.} \end{cases} \tag{39}$$

- P_{transfer} is the PDF associated with the transfer of cancer risk from the Japanese to United States population. A log-normal distribution function with an expectation value of 1 and geometric standard deviation of 1.3 was used, which corresponds to a 90% CI of 0.70 to 1.65 [3, 8].

- $P_{\text{Dosimetry}}$ is the PDF associated with estimates of bias and random errors in dosimetry. A normal distribution function with a mean value of 0.84 and a standard deviation of 0.11 was used. The standard deviation corresponds to a 90% CI from 0.69 to 1.0 [3, 8].

- $P_{\text{statistical}}$ is the PDF associated with the uncertainty of the risk coefficient, a parameter that takes into account the increase in risk with increasing radiation dose [8]. A normal distribution function with mean of 1 was used. The standard deviation of 0.15 corresponds to a 90% CI from 0.75 to 1.25 [3, 8].

- P_{Bias} is the PDF related to the error associated with the failure to detect cancer cases and the classification of cancer. A normal distribution function with a mean value of 1.1 and a standard deviation of 0.05 was used. The standard deviation corresponds to a 90% CI of 1.02 to 1.18 [3, 8].

The P_{Bias}, $P_{\text{Dosimetry}}$, P_{DDREF}, $P_{\text{statistical}}$,and P_{transfer} probability distribution functions for 20,000 Monte Carlo samples have been plotted in Figures 7-11. Each distribution has an associated quantile (random deviate) obtained by the Monte Carlo sampling procedure described in Appendix B. These quantiles are labeled χ_B for P_{Bias}, χ_D for $P_{\text{Dosimetry}}$, χ_{DDREF} for P_{DDREF}, χ_S for $P_{\text{statistical}}$,and χ_T for P_{transfer}. The product of the quantiles

gives χ_α in equation 22. For solid cancer [3],

$$\chi_\alpha^S = \frac{\chi_B \chi_D \chi_S \chi_T}{\chi_{\text{DDREF}}}, \tag{40}$$

and for leukemia,

$$\chi_\alpha^L = \chi_B \chi_D \chi_S \chi_T. \tag{41}$$

Note that the low-LET uncertainty is not reduced by the DDREF for leukemia, as the DDREF is only applied to linear models of dose response [8].

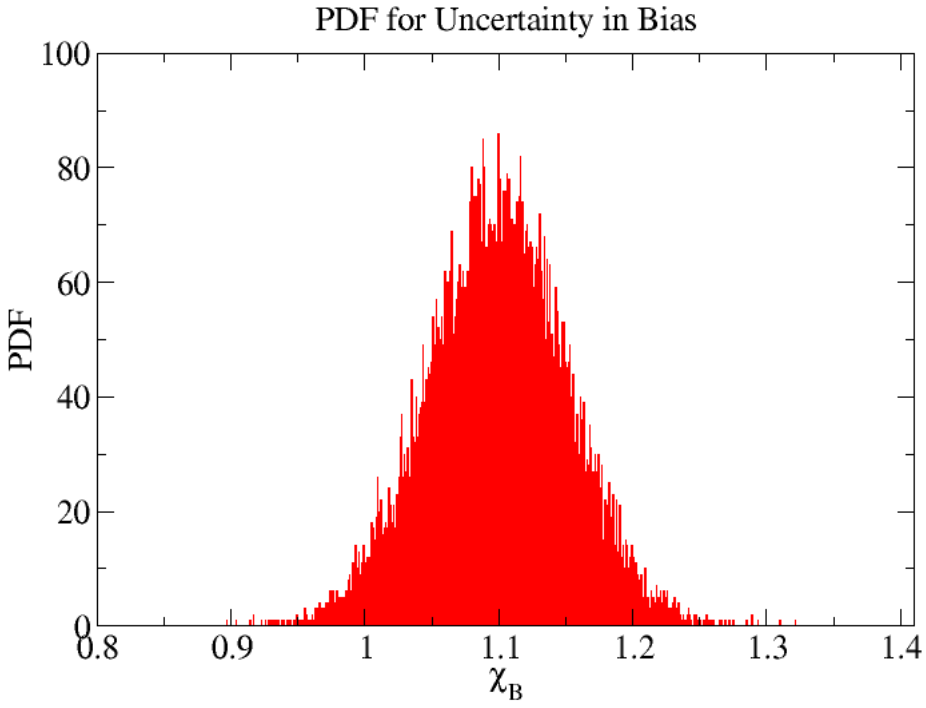

Figure 7: The p_{bias} Probability Distribution Function obtained from Monte Carlo sampling using 20,000 samples.

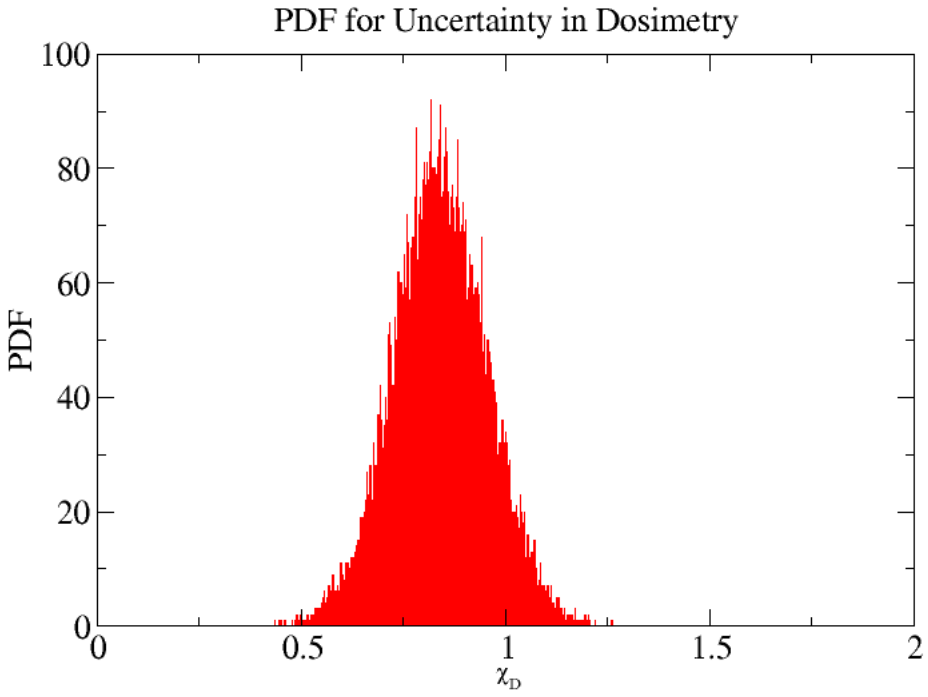

Figure 8: The $p_{\text{Dosimetry}}$ Probability Distribution Function obtained from Monte Carlo sampling using 20,000 samples.

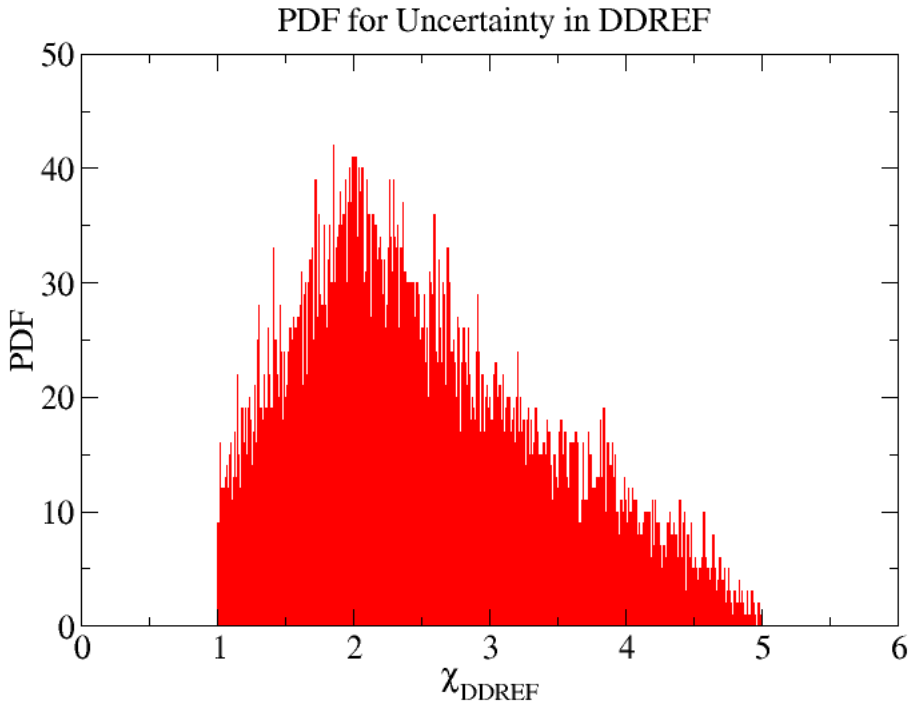

Figure 9: The p_{DDREF} Probability Distribution Function obtained from Monte Carlo sampling using 20,000 samples.

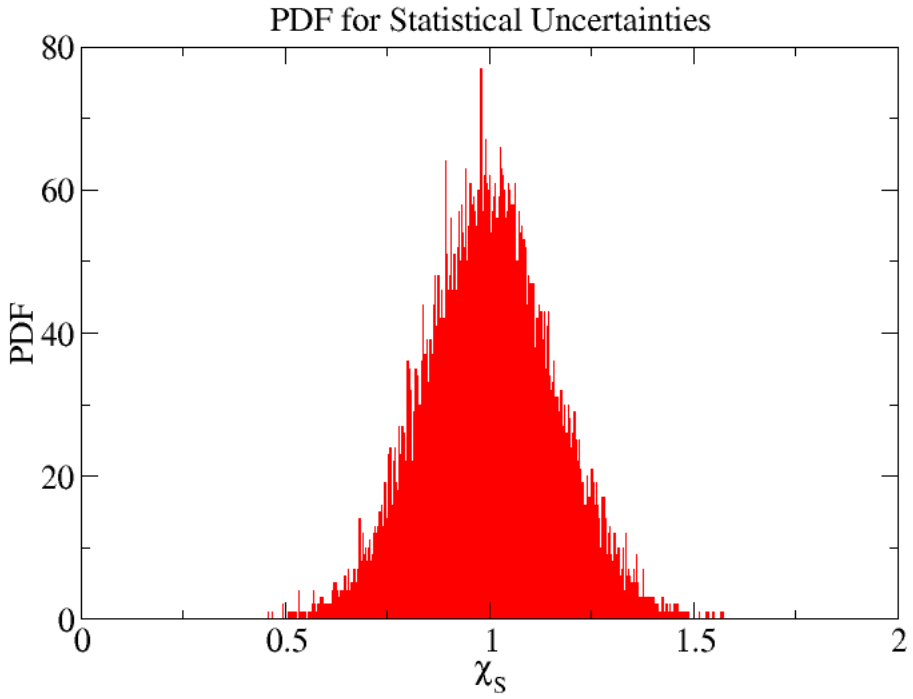

Figure 10: The $p_{\text{Statistical}}$ Probability Distribution Function obtained from Monte Carlo sampling using 20,000 samples.

3.3 Uncertainties in Physics

The uncertainty in fluence is projected to vary by ± 15% by Cucinotta et. al [3], though the actual uncertainty is not precisely known [14]. In the current work, a fluence uncertainty of ± 15% is assumed. For the uncertainty in fluence PDF, Cucinotta et al. [3] utilized normal distributions with a mean of $\mu = 0.65$ and LET dependent standard deviations: $\sigma = 1.0$ for LET ≤ 30 keV/μm, $\sigma = 2.0$ for 30 keV/μm $\leq$ LET ≤ 300 keV/μm, and $\sigma = 2.5$ for 300 LET $\geq$ keV/μm. In the current document, the physics uncertainty is modeled with Gaussian distributions with mean $\mu = 1$ and the following LET dependent standard deviations [3]:

$$\sigma(\text{LET}) = \begin{cases} 0.075 & \text{for} \quad \text{LET} < 30 \text{ keV}/\mu\text{m} \\ 0.150 & \text{for} \quad 30 \text{ keV}/\mu\text{m} \leq \text{LET} < 300 \text{ keV}/\mu\text{m} \\ 0.1875 & \text{for} \quad \text{LET} \geq 300 \text{ keV}/\mu\text{m} \end{cases} \tag{42}$$

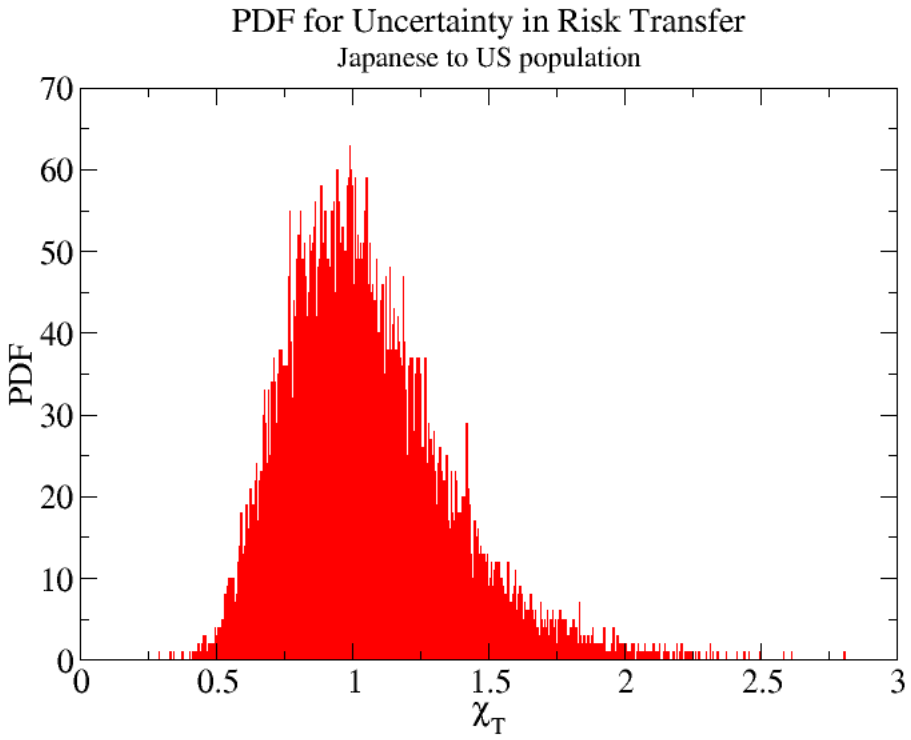

Figure 11: The p_{Transfer} Probability Distribution Function obtained from Monte Carlo sampling using 20,000 samples.

It is important to note that although this model was developed by Cucinotta et al. [3], the mean and standard deviations are significantly different from those reported in reference [3]. The probability distribution functions associated with uncertainty in physics are given in Figure 12.

4 Incorporating Uncertainty into Risk Calculations

This section describes how uncertainties are incorporated into the calculation of risk. In the last section, three uncertainties were identified that should be included in the calculation of the effective dose and the REID. These included uncertainties in the quality factor, fluence, and low LET risk model.

Quality factor uncertainties are incorporated by unique Monte Carlo sampling of the quality factor distribution functions described in the last section. For a given trial J, a unique quality factor is sampled. Figure 13 shows Monte Carlo samplings of the quality

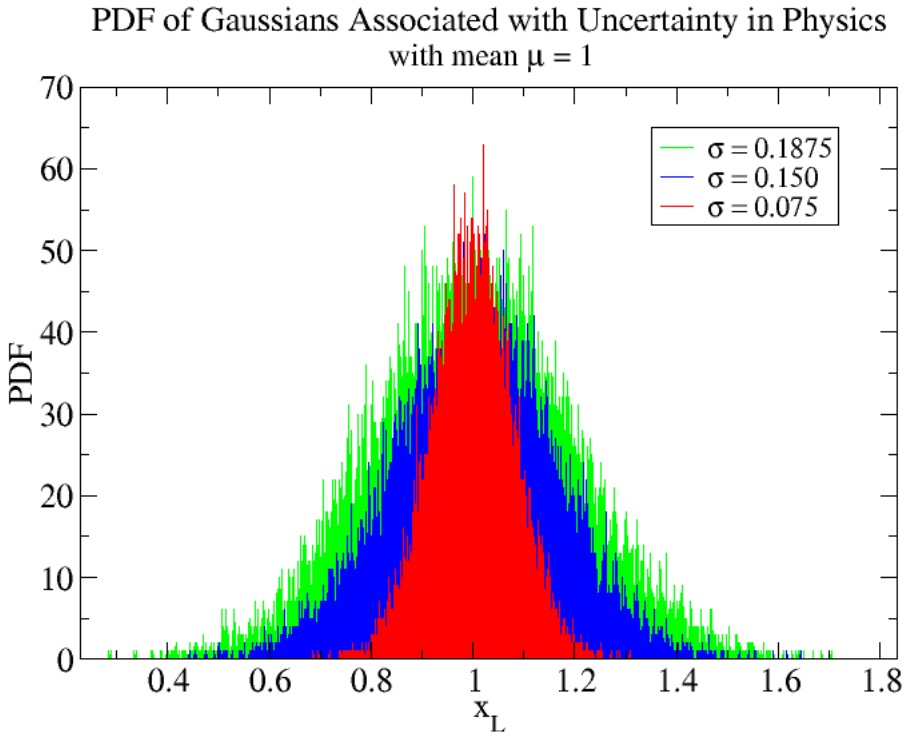

Figure 12: The PDF associated with uncertainties in fluence (physics) obtained with 20,000 Monte Carlo samples.

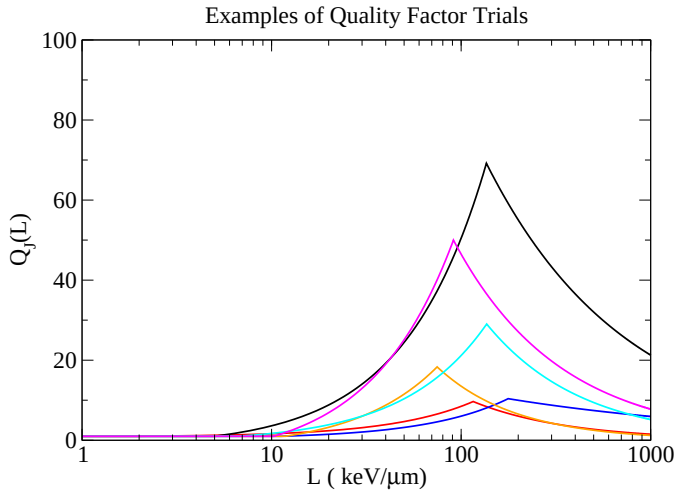

Figure 13: Monte Carlo samplings of the quality factor. These results are consistent with those given by [3].

factor and is consistent with the results of [3]. The quantiles (random deviates) associated with the fluence uncertainties are labeled as x_{LJ}, where L indicates that the quantile sampled depends on the LET region and J indicates the Monte Carlo trial. A full discussion of the Monte Carlo sampling techniques used in this document is found in Appendix B.

If the uncertainty in the quality factor and the fluence uncertainties are included in the effective dose, then equation (19) may be expressed as [3]

$$\mathrm{ED}_J = \sum_k \int_0^\infty F_k(E) L_k(E) Q_J(L_k(E)) x_{LJ} dE, \tag{43}$$

where k represents the sum over the ions in the radiation environment, and J indicates Monte Carlo samplings and is not a summing index, $F_k(E)$ is the tissue weighted fluence, $Q_J(L_k(E))$ is the quality factor, $L_k(E)$ is the LET, and x_{LJ} represents the fluence uncertainty.

Next, the low LET risk model uncertainties are included into the radiation cancer mortality rate in equation (22). For a trial J, the low LET risk model uncertainties are labeled as $\chi_{\alpha J}$. The radiation cancer mortality rate for a given Monte Carlo trial J may be written as [3]

$$m_J = m_0^S \chi_{\alpha J}^S + m_0^L \chi_{\alpha J}^L, \tag{44}$$

where m_0 is the baseline mortality rate described in the last section, $\chi_{\alpha J}$ is the quantile associated with the low LET uncertainty for a given Monte Carlo trial J, and S and L represent solid cancer and leukemia, respectively.

The REID is given as a function of radiation cancer mortality rate and exposed probability of survival [3, 5]

$$\text{REID}_J = \sum_{a=a_E}^{a_{max}} m_J(a, a_E, ED_J)\hat{S}_J(a, ED_J|a_E) \tag{45}$$

where a is the age, a_E is the age of exposure, ED is the effective dose, a_{max} is the maximum attained age (101 yr) [3], J represents a Monte Carlo trial, m_J is the radiation cancer mortality rate, and $\hat{S}_J(a, ED_J|a_E)$ is the radiation probability of survival given by [6]

$$\hat{S}_J(a, ED_J|a_E) = S_J(a, ED_J)/S_J(a_E, ED_J). \tag{46}$$

All of the equations given in the discussion of the effective dose and risk quantities, equations (11)-(14), will remain the same except $ED \to ED_J$, $\hat{S} \to \hat{S}_J$, $\tilde{S} \to \tilde{S}_J$, $q \to q_J$, and $m \to m_J$ to reflect the Monte Carlo sampling for the uncertainties.

5 Latency

Latency refers to the period of time elapsed after radiation exposure before any specific types of cancers are observed [8, 24]. The latency period is usually around two years for leukemia [9] and up to ten years for solid cancer [3]. A step-in latency model for both solid cancer and leukemia [3, 9] is utilized in the current work. This model is based on the Pierce et al. [9] LSS study. The Hiroshima atomic bomb event took place in 1945; however, the LSS does not include data taken before 1950. Since excess leukemias were observed two years after the atomic bomb, Pierce et al. [9] estimated that the EAR for the first five years after the 1945 exposure to be half of the EAR at 1950. After the step-in latency model has been used for the first five years following radiation exposure, the REID and other risk quantities may be calculated as usual.

6 Verification

Thus far, uncertainties in the quality factor, physics (fluence), and low LET uncertainties have been incorporated into the effective dose and the REID. In this section, the effect of the Monte Carlo sampling is shown.

The effective dose and the REID are generated for the August 1972 SPE [27], solar minimum GCR, and solar maximum GCR environments. The solar minimum environment was modeled using the dates October 26-28, 1976 with the Badhwar-O'Neill GCR model [28]. The solar maximum environment was modeled using a solar modulation parameter of 1110 MV with the Badhwar-O'Neill GCR model [28] as was done by [3]. All radiation transport was accomplished with HZETRN [20, 21, 22]. The fluxes generated from the

transport code are used for the effective dose and the REID calculations. In addition, the computerized anatomical female body model (CAF) has been used [29, 30]. Note that 600 day missions were used for the GCR environments, and all shielding materials discussed in this document are spherical shells.

6.1 Effective Dose

In order to verify the projected uncertainty in physics, the effective dose is calculated by sampling the physics uncertainty and by using the fixed ICRP 60 [12] definition of the quality factor. The physics uncertainty sampling produces a slightly asymmetric effective dose distribution, as seen in Figure 14. The median and 95% CI is given by 0.74 [0.62, 0.85] Sv for 40 yr females in a 20 g/cm^2 aluminum shield during a 600 day mission in the GCR solar minimum environment. The ratio of the 95% CI width to the median is used as a measure of the projected uncertainty from the median. In this example, the ratio is approximately 31%, which roughly produces the $\pm$15% uncertainty in the effective dose.

The uncertainties in physics and quality factor are included in the next calculation of the effective dose, which results in a log normal distribution. The effective dose for a 40 yr female in the GCR solar minimum environment under a 20 g/cm^2 shield is given in Figure 15. The median and 95% CI is 0.77 [0.47, 2.06] Sv. The probabilistic effective doses for aluminum, polyethylene, and titanium with 20 g/cm^2 and 5 g/cm^2 spherical shields for the GCR solar minimum (SOLAR MIN), GCR solar maximum (SOLAR MAX) and SPE environments are given in Table 2. A mission duration of 600 days was used for the GCR environments. Note that the effective dose is smaller in the GCR solar maximum environment than in the GCR solar minimum environment for thicker shields. This is expected, since the the GCR solar maximum environment has been modulated with a solar modulation parameter of 1100 MV. The thicker shields tend to mitigate SPE effectively. Thus, the contribution of the effective dose for thicker shielding is coming largely from the GCR environment, which has been modulated at solar maximum.

6.2 Risk

In this paper, three different ways of evaluating radiation risk have been examined: the REID, LAR, and ELR. The REID is the focus of this paper; however, the trends of the LAR and ELR curves are used to help confirm the results. In Figure 16, the REID, LAR, and ELR are plotted as a function of the effective dose. The low-LET risk uncertainty has not been included in this plot. The trends of the figure are consistent with the results of Kellerer et al. [4]. The LAR is larger than both the REID and the ELR. Furthermore, the REID is expected to be roughly 20% larger than the the ELR [4]. This is most notable at higher effective doses. There is little difference between all of the risk quantities at low effective doses. In Figure 17, the most probable values of the low LET uncertainty

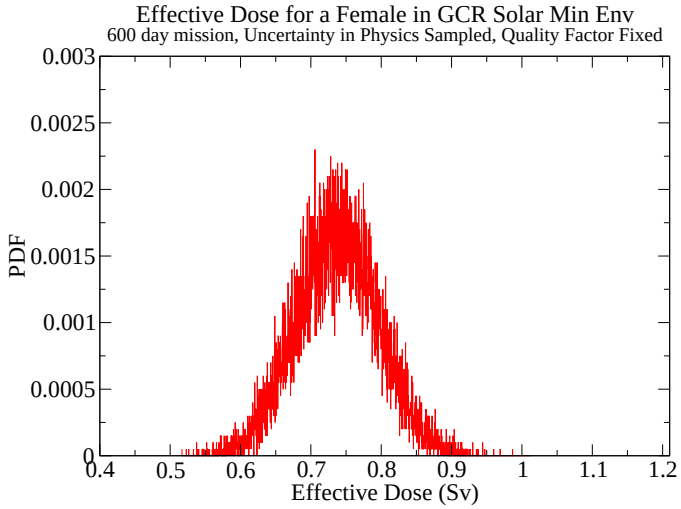

Figure 14: The effective dose for a female in a 20 g/cm^2 Al shield during a 600 day mission in the GCR solar minimum environment. The quality factor has been fixed to the ICRP 60 definition, but the uncertainty in physics has been sampled using Monte Carlo methods. The median and 95% CI is 0.74 [0.62, 0.85] Sv. See section 6 for a discussion of the GCR solar minimum environment.

distributions are included in the calculation of the risk as a function of effective dose, resulting in lower overall risk percentages.

Since the trend of the REID as a function of effective dose has been verified, the REID may be generated for each of the materials and thicknesses. Monte Carlo trials of the REID from equation (45) are binned into a histogram and are scaled by a factor of 100 to obtain the REID%. In Figure 18, the REID% for a 40 yr female in 20 g/cm^2 aluminum, polyethylene, and titanium shields during a 600 day mission in the GCR solar minimum environment has been generated. In Table 3, the REID% is calculated for aluminum, polyethylene, and titanium in the GCR solar minimum, GCR solar maximum, and SPE environments with 20 g/cm^2 and 5 g/cm^2 shields. A mission duration of 600 days was used for the GCR environments.

7 Material Analysis

The assessment of radiation shielding effectiveness based on material composition is an important concern for spacecraft design. In the current work, radiation shielding effectiveness is studied with percent difference distributions utilizing both correlated and uncorrelated uncertainties. In section 7.1, it is shown that the uncertainty of difference distributions may be reduced significantly when using correlated Monte Carlo samplings.

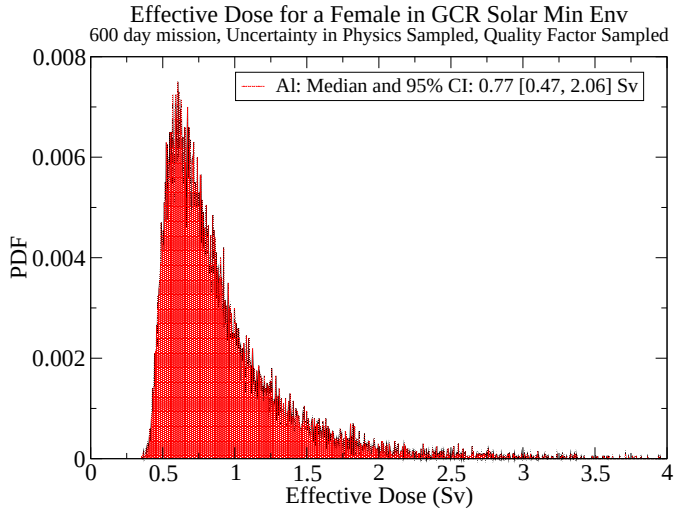

Figure 15: The effective dose for a female in a 20 g/cm^2 Al shield during a 600 day mission in the GCR solar minimum environment. Both the quality factor factor and the uncertainty in physics have been sampled. The median and 95% CI is 0.77 [0.47, 2.06] Sv. See section 6 for a discussion of the GCR solar minimum environment.

Table 2: Median Effective Dose and 95% CI for 20 g/cm^2 and 5 g/cm^2 aluminum (Al), polyethylene (Poly), and titanium (Ti) spherical shields. Note that smaller effective doses are expected more in the GCR solar maximum than GCR solar minimum environment for the thicker shields. This is due to the modulated GCR flux at solar maximum. See section 6 for a discussion of the GCR solar minimum (SOLAR MIN), GCR solar maximum (SOLAR MAX), and SPE space radiation environments. A mission duration of 600 days was used for the GCR environments.

	Effective Dose		
	SOLAR MIN	**SOLAR MAX**	**SPE**
Al (20 g/cm^2)	0.77 [0.47, 2.06] Sv	0.54 [0.35, 1.37] Sv	0.087 [0.067, 0.16] Sv
Al (5 g/cm^2)	0.93 [0.50, 0.78] Sv	1.26 [0.82, 3.13] Sv	0.72 [0.54, 1.54] Sv
Poly (20 g/cm^2)	0.66 [0.42, 1.67] Sv	0.42 [0.28, 1.03] Sv	0.040 [0.028, 0.087] Sv
Poly (5 g/cm^2)	0.86 [0.48, 2.53] Sv	0.97 [0.62, 2.47] Sv	0.48 [0.35, 1.01] Sv
Ti (20 g/cm^2)	0.85 [0.50, 2.32] Sv	0.59 [0.37, 1.50] Sv	0.13 [0.10, 0.24] Sv
Ti (5 g/cm^2)	0.93 [0.49, 2.79] Sv	1.26 [0.82, 3.13] Sv	0.73 [0.54, 1.55] Sv

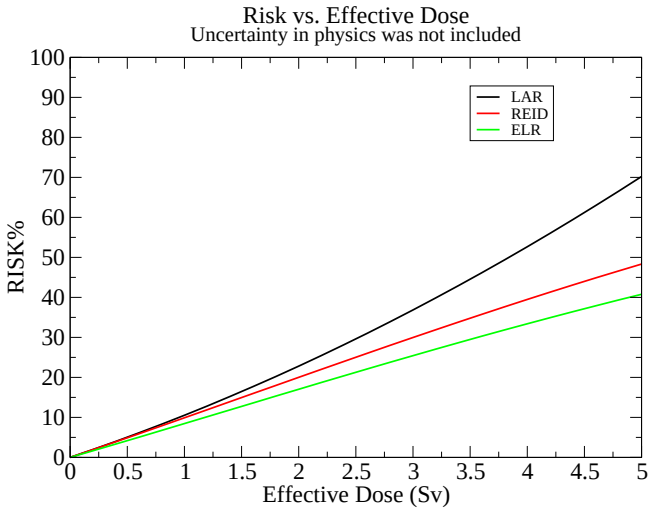

Figure 16: The LAR, REID, and ELR versus the effective dose. The low LET risk uncertainty has not been included here. These results show the correct trend for the three risk quantities. The LAR is expected to be larger than both the REID and the ELR, and the REID is expected to be roughly 20% larger than the ELR [4].

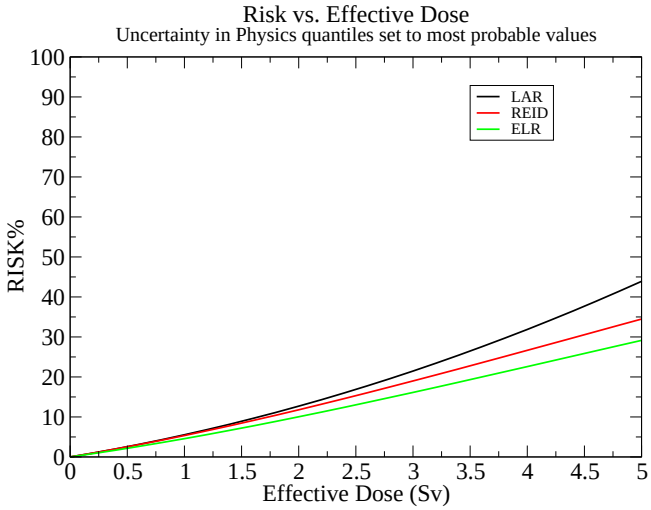

Figure 17: The LAR, REID, and ELR versus the effective dose. The most probable values of the low LET uncertainty distributions have been included. These results show the correct trend for the three risk quantities. The LAR is expected to be larger than both the REID and the ELR, and the REID is expected to be roughly 20% larger than the ELR [4].

Table 3: Median REID% and 95% CI for 20 g/cm^2 and 5 g/cm^2 aluminum (Al), polyethylene (Poly), and titanium (Ti) spherical shields. Note that smaller REID% are expected (as a result of smaller effectives doses) in the GCR solar maximum than GCR solar minimum environment for the thicker shields. This is due to the modulated GCR flux at solar maximum. See section 6 for a discussion of the GCR solar minimum (SOLAR MIN), GCR solar maximum (SOLAR MAX), and SPE space radiation environments. A mission duration of 600 days was used for the GCR environments.

	REID		
	SOLAR MIN	**SOLAR MAX**	**SPE**
Al (20 g/cm^2)	3.40% [1.90%, 10.90%]	2.30% [1.34%, 6.40%]	0.34% [0.25%, 0.63%]
Al (5 g/cm^2)	4.20% [2.05%, 15.68%]	5.98% [3.57%, 18.28%]	3.19% [2.22%, 7.54%]
Poly (20 g/cm^2)	2.87% [1.72%, 8.38%]	1.76% [1.09%, 4.79%]	0.15% [0.10%, 0.34%]
Poly (5 g/cm^2)	3.87% [1.96%, 14.01%]	4.39% [2.62%, 13.63%]	2.00% [1.40%, 4.63%]
Ti (20 g/cm^2)	3.77% [2.09%, 12.46%]	2.53% [1.49%, 7.39%]	0.53% [0.39%, 0.98%]
Ti (5 g/cm^2)	4.20% [2.05%, 15.73%]	5.99% [3.59%, 18.41%]	3.19% [2.20%, 7.63%]

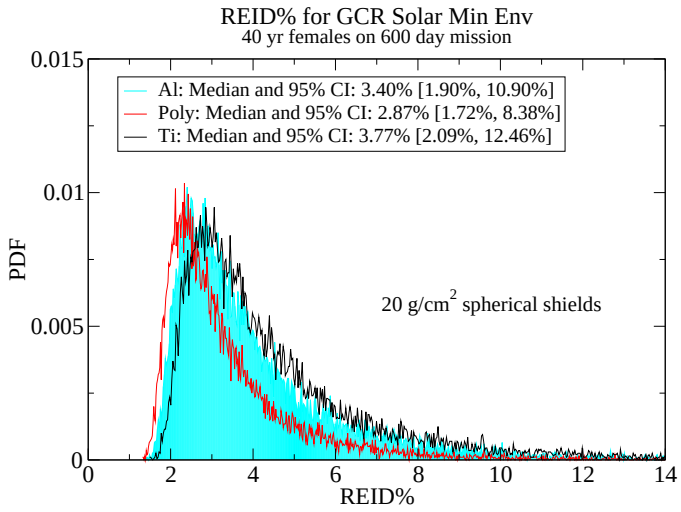

Figure 18: The REID% for a 40 yr female in spherical 20 g/cm^2 aluminum (Al), polyethylene (Poly), and titanium (Ti) shields on a 600 day mission in the GCR solar minimum environment.

Furthermore, the use of uncorrelated distributions introduces extraneous uncertainty in the difference of distributions when interdependence is clearly established.

In a recent study, Cucinotta et al. [3] showed that polyethylene and carbon shields do not significantly reduce the risk as compared to aluminum. This was attributed to large radiobiological uncertainties that tend to dominate over other uncertainties. Reference [3] used a χ^2 analysis based on the assumption that the quality factor and low LET uncertainties for different materials were uncorrelated. However, the quality factor and the low LET uncertainties depend on LET only; there is no dependence on material composition. Therefore, the use of independent Monte Carlo samplings of the quality factor and low-LET uncertainty for two different materials introduces extraneous uncertainty in the percent difference of the effective dose and the REID distributions. Consequently, correlated quality factors and low LET uncertainties should be considered in evaluating shielding effectiveness.

In sections 7.2 and 7.3, correlated quality factors are shown to significantly reduce the uncertainty of the percent difference as compared to uncorrelated quality factors. The same approach is taken for correlated low LET uncertainties, where only a modest reduction of the percent difference uncertainty is achieved.

7.1 Correlative Effects on Uncertainty

In this section, the effect of using uncorrelated and correlated Monte Carlo samplings in the difference of distributions is discussed. The reader is directed to Appendix B for a full discussion of Monte Carlo sampling techniques.

Let two distributions be defined by the following sets:

$$f(x) = \{x_1^f, x_2^f, x_3^f, \ldots, x_N^f\} \tag{47}$$

and

$$g(x) = \{x_1^g, x_2^g, x_3^g, \ldots, x_N^g\}, \tag{48}$$

where x_i^f are the x-deviates of the $f(x)$ distribution, and x_i^g are the x-deviates of the $g(x)$ distribution; N is the total number of deviates in the set. The difference of the two distributions, $D = f(x) - g(x)$, is obtained by subtracting the elements:

$$D = \{x_1^f - x_1^g, x_2^f - x_2^g, \ldots, x_N^f - x_N^g\}. \tag{49}$$

Next, let $f^1(x)$ and $f^2(x)$ denote two independently sampled distributions constructed from the same function. Then, the difference $D = f^1(x) - f^2(x)$ is expressed as

$$D = \{x_1^{1f} - x_1^{2f}, x_2^{1f} - x_2^{2f}, \ldots x_N^{1f} - x_N^{2f}\}. \tag{50}$$

An example of such a difference is illustrated for a normal distribution in Figure 19,

$$f(x) = \frac{1}{\sqrt{2\pi\sigma^2}} \exp\left[\frac{-(x-\mu)^2}{2\sigma^2}\right], \tag{51}$$

where $\mu = 2$ and $\sigma = 1$. The median and 95% CI of the difference of the two distributions is given by 0.0088 [-2.68, 2.68]. In this example, the Monte Carlo samplings have no interdependence and may be viewed as being uncorrelated. If a single Monte Carlo sampling of the distribution is used, then the median and 95% CI is obviously 0.0 [0.0, 0.0]. In this case, there is obvious interdependence, or correlation, because the same sampling of the distribution was used in the difference. The use of correlated Monte Carlo samplings allows for the reduction of uncertainty in the difference.

Suppose that the difference involves a product of distributions, such as

$$D = f^1(x)g(x) - f^2(x)h(x) \tag{52}$$

where $f(x)$, $g(x)$, and $h(x)$ are distributions, and the superscripts on $f(x)$ indicate independent Monte Carlo samplings. If a correlated Monte Carlo sampling of the $f(x)$ distribution is used, then $f^1(x) = f^2(x) = f(x)$, and

$$D = f(x)g(x) - f(x)h(x) = f(x)\Big[g(x) - h(x)\Big] \tag{53}$$

In this case, the result could be attributed to differences in the $g(x)$ and $h(x)$ distributions rather than independent samplings of the same distribution function $f(x)$, and the overall uncertainty in the difference would be reduced. This is best illustrated with an example. Consider the following difference in distributions

$$D = f_2^1(x)f_3(x) - f_2^2(x)f_1(x), \tag{54}$$

where $f_\mu(x)$ are distributions sampled from equation (51) and μ is the mean. The superscripts represent unique Monte Carlo samplings of the same function. The standard deviation is set to 1 for each distribution. The difference defined in equation (54) is expected to have a median of 4, based on the most probable values of the normal distributions. The uncorrelated difference is represented by the red distribution in Figure 20, where the median and 95% CI is given by 3.40 [-6.99, 9.50]. If correlated Monte Carlo samplings are used in the difference, then $f_2^1 = f_2^2$ in equation (54), and the median and 95% CI is given by 4.07 [0.16, 8.10]. This is illustrated by the blue curve in Figure 20. These examples show that the use of uncorrelated Monte Carlo samplings introduces extraneous uncertainty in the difference of distributions. In addition, the use of uncorrelated Monte Carlo samplings led to skewing of the median from the most probable result.

Note that the difference in equation (52) was chosen because it is analogous to the

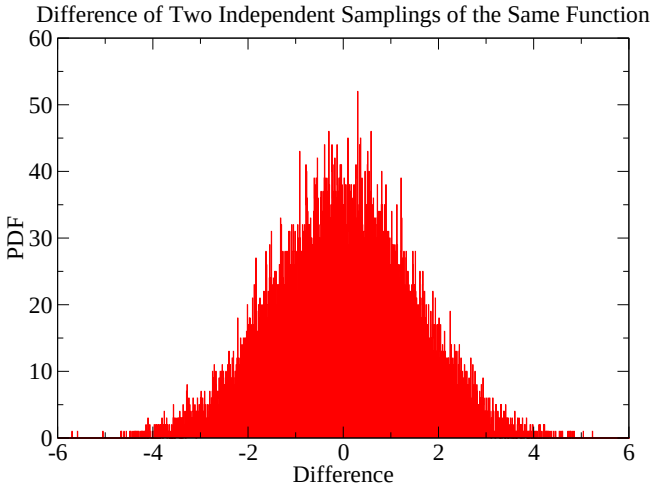

Figure 19: The difference of two independently sampled distributions of a single function.

effective dose difference distribution that follows in the next section. In this context, the quality factor is associated with the discussion of f_2^1 and f_2^2 above. The fact that integrals are involved has no bearing on the argument.

7.2 Effective Dose

The percent difference for the effective dose distributions of two materials is expressed as

$$\%\mathrm{DIFF}_{\mathrm{ED}} = \frac{\mathrm{ED}_1 - \mathrm{ED}_2}{(\mathrm{ED}_1 + \mathrm{ED}_2)/2} \times 100, \tag{55}$$

where ED is the probabilistic effective dose distribution given by equation (43), and the subscript indicates a material label. The uncorrelated difference of the effective dose distributions for two materials is written as

$$\begin{aligned} \mathrm{ED}_1 - \mathrm{ED}_2 = & \\ & \sum_k \int_0^\infty F_k^1(E) L_k^1(E) Q_J^1(L_k^1(E)) x_{LJ}^1 dE \\ & - \sum_k \int_0^\infty F_k^2(E) L_k^2(E) Q_J^2(L_k^2(E)) x_{LJ}^2 dE, \end{aligned} \tag{56}$$

where k is the summation index for the ions, the superscripts represent material labels and unique Monte Carlo samplings, $F_k(E)$ is the fluence, $L_k(E)$ is the linear energy transfer,

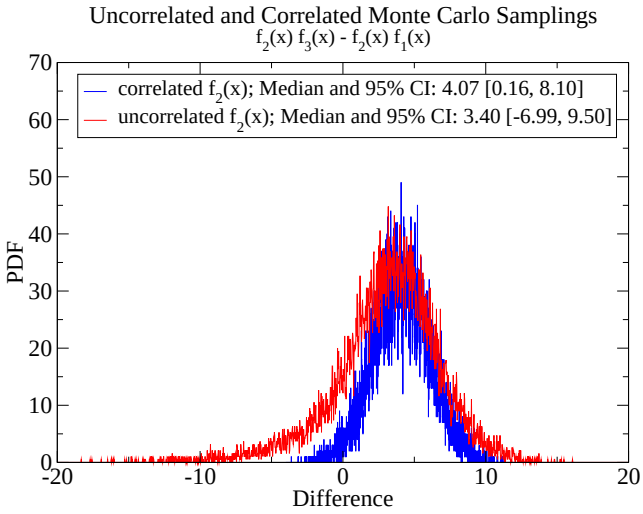

Figure 20: The effect of using correlated distributions is shown to reduce the uncertainty in difference of distributions.

$Q_J(L(E))$ is the quality factor, and x_{LJ} is the uncertainty in physics.

Since the quality factor is independent of material composition, correlated quality factors should be used for the percent difference. Using the correlated quality factor, the effective dose difference may be expressed as

$$\begin{aligned} &\mathrm{ED}_1 - \mathrm{ED}_2 = \\ &\sum_k \int_0^\infty [Q_J(L_k^1(E))F_k^1(E)L_k^1(E)x_{LJ}^1 \\ &- Q_J(L_k^2(E))F_k^2(E)L_k^2(E)x_{LJ}^2]dE. \end{aligned} \tag{57}$$

In equation (56), Q_J^1 and Q_J^2 represent two unique samplings of the quality factor for a single Monte Carlo trial. Each unique sampling corresponds to a unique functional form of the quality factor. However, for the correlated difference given by equation (57), the functional form of the quality factor Q_J is obtained once per Monte Carlo trial. Thus, a single functional form of the quality factor is used for the difference per trial. Using the effective dose distribution differences in equations (56) and (57) and similar effective dose distribution sums, the percent difference of the effective dose distributions is calculated.

In Figure 21, the percent difference of the effective doses is plotted for aluminum and polyethylene during a 600 day mission in the GCR solar maximum environment as calculated with uncorrelated and correlated quality factors. The percent difference was calculated using equation (55) with $\mathrm{ED}_1 = \mathrm{ED}_{\mathrm{Al}}$ and $\mathrm{ED}_2 = \mathrm{ED}_{\mathrm{Poly}}$, where $\mathrm{ED}_{\mathrm{Al}}$ is

the effective dose distribution of aluminum and $\mathrm{ED}_{\mathrm{Poly}}$ is the effective dose distribution of polyethylene. Positive percent difference values indicate a larger effective dose for aluminum than polyethylene, whereas negative percent difference values indicate a larger effective dose for polyethylene than aluminum. The initial calculation of the percent difference with uncorrelated quality factors results in a median and 95% CI of 6.25% [-18.29%, 27.91%]. Since much of the confidence interval is negative, it is difficult to discern if the effective dose for aluminum is actually larger than than that of polyethylene. After using the correlated quality factor, the median changes only slightly to 6.03%; however, the 95% CI is reduced significantly to [0.43%, 11.79%]. Since the 95% CI of the percent difference distribution is positive, one may assert with much higher confidence that the effective dose percent difference of aluminum is greater than that of polyethylene. In Table 4, the effective dose differences for aluminum, polyethylene, and titanium for 20 g/cm^2 and 5 g/cm^2 spherical shields are calculated for the different radiation environments. A mission duration of 600 days was used for the GCR environments. There are some cases in which the lower bound of the 95% confidence interval is negative after using correlated quality factors and correlated low LET uncertainties. In these cases, the confidence interval that gives the minimum positive bound was found when the median was significantly different from zero and positive. The median may also be statistically different from zero and negative. If this occurs, the confidence interval that gives the upper negative bound is found.

In the next section, the percent difference of the REID distributions for different materials is examined.

7.3 REID

In the last section, the effect of using a correlated quality factor distributions was to reduce the uncertainty in the percent difference of the effective dose for two materials. Since the REID is a function of effective dose, the correlated quality factors must again be considered. In addition, the REID is proportional to the low LET uncertainty through the radiation cancer mortality rate m_J from equation (44).

The percent difference of two REID distributions for two different materials is given by

$$\%\mathrm{DIFF}_{\mathrm{REID}} = \frac{\mathrm{REID}_1 - \mathrm{REID}_2}{(\mathrm{REID}_1 + \mathrm{REID}_2)/2} \times 100, \tag{58}$$

where the REID is given by equation (45). The REID also includes deviates associated with low LET uncertainty, x_{LJ}, where L represents the low LET uncertainty and J represents a Monte Carlo trial. The uncorrelated difference of two REID distributions is

Table 4: The effective dose percent difference distributions for aluminum (Al), polyethylene (Poly), and titanium (Ti) as calculated with equation 55. Unless otherwise stated, all confidence intervals are 95%. See section 6 for a discussion of the GCR solar minimum (SOLAR MIN), GCR solar maximum (SOLAR MAX), and SPE space radiation environments. A mission duration of 600 days was used for the GCR environments.

	Effective Dose % Difference		
	SOLAR MIN	**SOLAR MAX**	**SPE**
Al/Poly (20 g/cm^2)			
Uncorr. Q	3.54% [-20.76%, 27.34%]	6.25% [-18.29%, 27.91%]	18.79% [-0.13%, 31.09%]
Corr. Q	3.65% [-1.83%, 9.77%]	6.03% [0.43%, 11.79%]	18.44% [11.79%, 23.26%]
Corr. Q (81% CI)	3.65% [0.037%, 7.56%]	–	–
Al/Poly (5 g/cm^2)			
Uncorr. Q	1.96% [-25.98%, 29.38%]	6.65% [-13.76%, 24.64%]	10.51% [-8.91%, 27.32%]
Corr. Q	1.76% [-4.14%, 8.03%]	6.58% [2.51%, 10.44%]	10.46% [5.76%, 16.97%]
Corr. Q (44% CI)	1.76% [0.033%, 3.53%]	–	–
Ti/Al (20 g/cm^2)			
Uncorr. Q	2.31% [-23.65%, 27.11%]	1.95% [-21.74%, 25.26%]	10.62% [-5.09%, 24.26%]
Corr. Q	2.33% [-3.18%, 8.06%]	2.16% [-2.78%, 7.37%]	10.65% [5.81%, 15.33%]
Corr. Q (60% CI)	2.33% [0.018%, 4.68%]	–	–
Corr. Q (62% CI)	–	2.16% [0.022%, 4.34%]	–
Ti/Al (5 g/cm^2)			
Uncorr. Q	-0.19% [-28.55%, 28.40%]	-0.024% [-18.88%, 18.60%]	-0.11% [-19.09%, 18.72%]
Corr. Q	-0.0035% [-6.10%, 6.00%]	0.014% [-2.81%, 2.85%]	0.0048% [-4.74%, 4.69%]
Ti/Poly (20 g/cm^2)			
Uncorr. Q	5.85% [-19.17%, 29.22%]	8.19% [-16.51%, 29.71%]	27.29% [10.47%, 36.87%]
Corr. Q	6.00% [0.46%, 12.25%]	8.17% [2.55%, 14.00%]	26.94% [21.48%, 30.74%]
Ti/Poly (5 g/cm^2)			
Uncorr. Q	1.81% [-26.30%, 28.77%]	6.66% [-13.67%, 24.16%]	10.47% [-9.00%, 26.99%]
Corr. Q	1.76 % [-4.17%, 8.01%]	6.59% [2.50%, 10.45%]	10.47% [5.77%, 14.97%]
Corr. Q (45% CI)	1.76% [0.0031%, 3.55%]	–	–

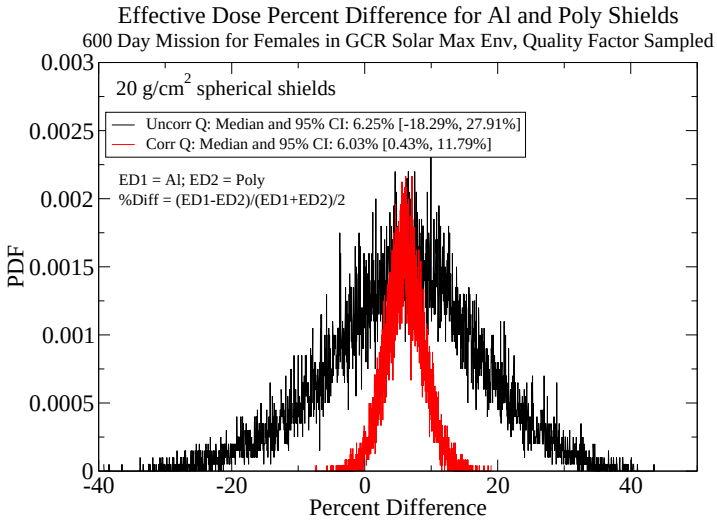

Figure 21: The percent difference of the effective doses for aluminum (Al) and polyethylene (Poly) during a 600 day mission in the GCR solar maximum environment as calculated with uncorrelated and correlated quality factors. The 95% CI reduces significantly after using correlated quality factors. See section 6 for a discussion of the GCR solar maximum environment.

given by

$$\begin{aligned} &\mathrm{REID}_1 - \mathrm{REID}_2 = \\ &\sum_{\mathrm{a=a_E}}^{a_{max}} m_J^1(a, a_E, ED_J^1)\hat{S}_J(a, ED_J^1(Q_J^1)|a_E) \\ &- \sum_{a=a_E}^{a_{max}} m_J^2(a, a_E, ED_J^2)\hat{S}_J(a, ED_J^2(Q_J^2)|a_E) \end{aligned} \tag{59}$$

where superscripts represent material label and unique Monte Carlo samplings, ED_J^1 and ED_J^2 are the uncorrelated effective doses, Q_J^1 and Q_J^2 are independent samplings of the quality factors per trial J, and m_J^1 and m_J^2 are the uncorrelated radiation cancer mortality rates.

The low LET uncertainties should be treated as correlated, since the low LET uncertainty has no dependence on the material. Using both correlated effective doses and

correlated low LET uncertainties, the difference becomes

$$\begin{aligned}&\mathrm{REID}_1 - \mathrm{REID}_2 = \\ &\sum_{a=a_E}^{a_{max}} [m_J(a, a_E, ED_J^1)\hat{S}_J(a, ED_J^1(Q_J)|a_E) \\ &- m_J(a, a_E, ED_J^2)\hat{S}_J(a, ED_J^2(Q_J)|a_E)]\end{aligned} \tag{60}$$

where m_J represents the correlated low LET uncertainty sampling for the radiation cancer mortality for both materials, and Q_J represents a correlated quality factor for both materials.

The percent difference of the REID distributions for 40 yr females behind 20 g/cm^2 spherical aluminum and polyethylene shields during a 600 day mission in the GCR solar maximum environment is given in Figure 22. The medians and 95% CIs have been listed in each case. In the first case, both uncorrelated quality factors and uncorrelated low LET uncertainties have been used for the percent difference. This results in a distribution with a broad 95% CI, which makes it difficult to distinguish which material poses greater risk. In the next case, a correlated quality factor has been used with uncorrelated low-LET uncertainties. This reduces the 95% confidence interval significantly. However, there is still some uncertainty in which material poses greater risk. The reason for this is that the lower bound on the 95% CI is negative, which implies a chance that polyethylene may pose greater risk than aluminum. Finally, both correlated quality factors and correlated low LET uncertainties are used to calculate the percent difference. Since the upper and lower bounds of the 95% CI are positive, it may be stated with 95% confidence that aluminum poses 6.57% greater risk than polyethylene.

In Table 5, the percent differences of the REID distributions for aluminum, polyethylene, and titanium for 40 yr females behind 20 g/cm^2 and 5 g/cm^2 spherical shields are calculated during 600 day missions in different radiation environments using correlated and uncorrelated uncertainties. The median and 95% CI for each case has been listed. There are some cases in which the lower bound of the 95% CI is negative after using correlated quality factors and correlated low LET uncertainties. In these cases, the confidence interval that gives the minimum positive bound was found when the median was significantly different from zero. The median may also be statistically different from zero and negative. If this occurs, the confidence interval that gives the upper negative bound is found. Correlated uncertainties in quality factor and physics are used in the discussion that follows.

The percent difference of the REID for a 40 yr female in 20 g/cm^2 and 5 g/cm^2 spherical aluminum and polyethylene shields. With the use of correlated quality factor and physics uncertainties, it may be stated with 95% confidence that aluminum poses greater risk than polyethylene during the SPE and GCR solar maximum environments for both 5 g/cm^2 and 20 g/cm^2 shield thicknesses. During the GCR solar minimum, it is

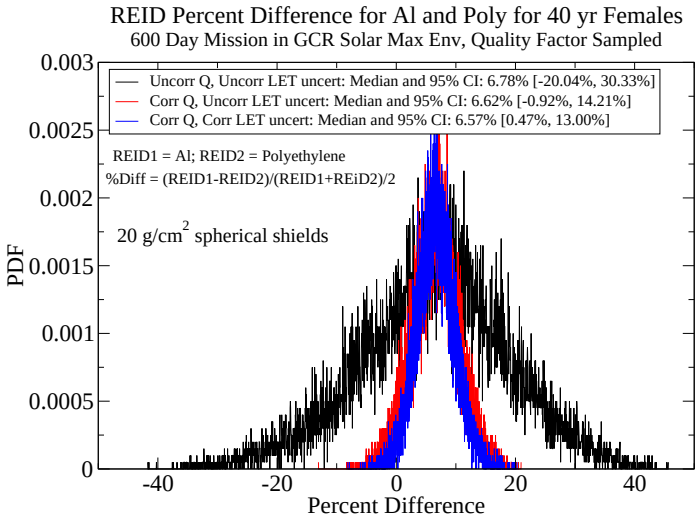

Figure 22: The percent difference of the REID distributions for a 40 yr female behind aluminum (Al) and polyethylene (Poly) spherical shields during a 600 day mission in the GCR solar maximum environment as calculated with uncorrelated and correlated uncertainties. The 95% CI is reduced significantly after using correlated quality factors. However, there is still some uncertainty in which material poses greater risk. After including correlated low LET uncertainties, aluminum can be identified with 95% confidence to pose greater risk than polyethylene. See section 6 for a discussion of the GCR solar maximum environment.

predicted with 81% confidence that aluminum poses greater risk than polyethylene in the 20 g/cm^2 shield. However, the REID percent difference for aluminum and polyethylene is 2.01% [0.036%, 4.05%] with 44% confidence for the GCR solar minimum environment in the 5 g/cm^2 shield.

As shown in Table 5, it can be stated with approximately 60% confidence that titanium poses greater risk than aluminum in the 20 g/cm^2 shield for the GCR solar minimum and maximum environments. In addition, when an SPE event is considered, titanium is shown to pose 10.83% [5.86%, 15.67%] greater risk than aluminum in the thicker shield. There is no statistical difference between the titanium and aluminum shields in mitigating the risk for the thinner shield of 5 g/cm^2.

It is also shown in Table 5 with 95% confidence that titanium poses greater risk than polyethylene for the GCR solar minimum, GCR solar maximum, and SPE environments in the 20 g/cm^2 shield. In the 5 g/cm^2, titanium poses greater risk than aluminum for the GCR solar maximum and SPE environments. However, it may only be stated with 45% confidence that titanium poses greater risk than polyethylene in the 5 g/cm^2 shield.

Table 5: The REID percent difference distributions for aluminum (Al), polyethylene (Poly), and titanium (Ti) as calculated with equation 55. Unless otherwise stated, all confidence intervals are 95%. See section 6 for a discussion of the GCR solar minimum (SOLAR MIN), GCR solar maximum (SOLAR MAX), and SPE space radiation environments. A mission duration of 600 days was used for the GCR environments.

	REID % Difference		
	SOLAR MIN	**SOLAR MAX**	**SPE**
Al/Poly (20 g/cm^2)			
Uncorr. Q, Uncorr. χ_L	4.00% [-23.53%, 30.61%]	6.78% [-20.04%, 30.33%]	18.92% [-0.67%, 31.74%]
Corr. Q, Uncorr. χ_L	4.17% [-3.56%, 12.33%]	6.62% [-0.92%, 14.21%]	18.55% [10.61%, 24.83%]
Corr. Q, Corr. χ_L	4.10% [-2.05%, 11.27%]	6.57% [0.47%, 13.00%]	18.64% [12.00%, 23.47%]
Corr. Q, Corr. χ_L (81% CI)	4.10% [0.042%, 8.63%]	–	–
Al/Poly (5 g/cm^2)			
Uncorr. Q, Uncorr. χ_L	2.06% [-29.68%, 33.06%]	7.77% [-16.71%, 28.58%]	11.45% [-10.29%, 30.12%]
Corr. Q, Uncorr. χ_L	2.03% [-5.87%, 10.41%]	7.64% [1.40%, 13.70%]	11.60% [4.78%, 18.02%]
Corr. Q, Corr. χ_L	2.01% [-4.79%, 9.39%]	7.67% [2.98%, 12.14%]	11.55% [6.35%, 16.51%]
Corr. Q, Corr. χ_L (44% CI)	2.01% [0.036%, 4.05%]	–	–
Ti/Al (20 g/cm^2)			
Uncorr. Q, Uncorr. χ_L	2.58% [-27.08%, 30.65%]	2.18% [-24.31%, 28.05%]	10.84% [-5.86%, 25.36%]
Corr. Q, Uncorr. χ_L	2.63% [-5.04%, 10.46%]	2.42% [-4.71%, 9.60%]	10.82% [3.98%, 17.47%]
Corr. Q, Corr. χ_L	2.64% [-3.61%, 9.32%]	2.37% [-3.11%, 8.33%]	10.83% [5.86%, 15.67%]
Corr. Q, Corr. χ_L (60% CI)	2.64% [0.029%, 5.32%]	–	–
Corr. Q, Corr. χ_L (62% CI)	–	2.37% [0.026%, 4.82%]	–
Ti/Al (5 g/cm^2)			
Uncorr. Q, Uncorr. χ_L	-0.27% [-32.42%, 32.02%]	0.034% [-22.47%, 22.32%]	-0.048% [-21.68%, 21.37%]
Corr. Q, Uncorr. χ_L	0.017% [-8.19%, 8.19%]	0.0074% [-5.17%, 5.24%]	0.0019% [-6.99%, 7.00%]
Corr. Q, Corr. χ_L	-0.0034% [-7.11%, 6.99%]	0.016% [-3.37%, 3.43%]	-0.0072% [-5.41%, 5.37%]
Ti/Poly (20 g/cm^2)			
Uncorr. Q, Uncorr. χ_L	6.58% [-22.24%, 32.70%]	8.86% [-18.31%, 32.33%]	27.52% [10.22%, 37.40%]
Corr. Q, Uncorr. χ_L	6.75% [-0.94%, 15.09%]	8.94% [1.32%, 16.65%]	27.21% [20.74%, 32.20%]
Corr. Q, Corr. χ_L	6.74% [0.51%, 14.26%]	8.91% [2.81%, 15.55%]	27.26% [21.86%, 31.05%]
Ti/Poly (5 g/cm^2)			
Uncorr. Q, Uncorr. χ_L	2.06% [-29.93%, 32.64%]	7.63% [-16.40%, 27.90%]	11.45% [-10.60%, 29.90%]
Corr. Q, Uncorr. χ_L	2.04% [-6.05%, 10.53%]	7.66% [-1.48%, 13.58%]	11.60% [4.63%, 18.00%]
Corr. Q, Corr. χ_L	2.02% [-4.82%, 9.43%]	7.69% [2.97%, 12.17%]	11.55% [6.25%, 16.56%]
Corr. Q, Corr. χ_L (45% CI)	2.02% [0.0039%, 4.08%]	–	–

8 Conclusions

The largest source of uncertainty in radiation risk assessment is the quality factor due to lack of experimental data for the energy and ions of interest in the space radiation environment. Consequently, determining optimal shielding materials that reduce the REID in a statistically significant manner has been found to be difficult in previous studies.

In the current work, it is demonstrated that correlated uncertainties may be used to reduce the overall uncertainty in the difference of distributions. Moreover, the use of uncorrelated uncertainties is shown to introduce extraneous uncertainty in the difference of distributions when clear correlation (interdependence) is established. Since the quality factor used in the current work is independent of material composition, correlated quality factors should be used when evaluating the difference of the REID distributions.

The effect of composition on shielding effectiveness is studied with the difference of the REID distributions for different materials. It is shown, with the use of correlated uncertainties, that statistically significant differences between materials can be determined despite the large uncertainties in the quality factor. This differs from previous studies where uncertainties have been generally treated as uncorrelated. It is concluded that the use of correlated quality factor uncertainties significantly reduces the uncertainty in the assessment of shielding effectiveness for the mitigation of radiation exposure.

Appendices

A Life Tables

In this document, the background mortality rate for all causes of death $M(a)$ and the solid cancer mortality rate $m_c^S(a)$ are used. The background mortality rate for all causes of death is taken from the National Vital Statistics Reports (NVSR) [15]. Mortality data are usually given in the form of life tables. (See Shryock [31] and Chiang [32] for useful discussions of life tables.) The first six years of the relevant columns from the background mortality life table have been listed in Table 6. The mortality rate is calculated by dividing the number of people dying in the time interval by the number living in the same time interval.

The probability of survival may be calculated from mortality rates with equations (7) and (8). The background mortality rate for all causes of death is plotted in Figure 23. The probability of death can be calculated from noting that the probability of survival plus the probability of death is 1. It is important to distinguish the probability of dying in an age interval, q_γ in equation (7), from the probability of death. The probability of death may be expressed in a form that is analogous to equation (8), which involves a product of $q_\gamma(a)$ from birth to some maximum age, $\mathrm{a_{max}}$. The probability of death during

Table 6: A portion of the unabridged Background Mortality Table for all causes of death for Males. The background cancer mortality rate $M(a)$ is obtained by dividing the number dying in an age interval by the number of people years lived in the same time interval.

Age at Death (yr)	Number Dying in (a,a+1)	Number of PY lived in (a,a+1) [PY]	Background Mortality Rate: M(a) $[PY]^{-1}$
0-1	759	99333	0.0076409
1-2	56	99213	0.0005644
2-3	38	99165	0.0003832
3-4	28	99132	0.0002823
4-5	22	99107	0.0002220
5-6	21	99086	0.0002119

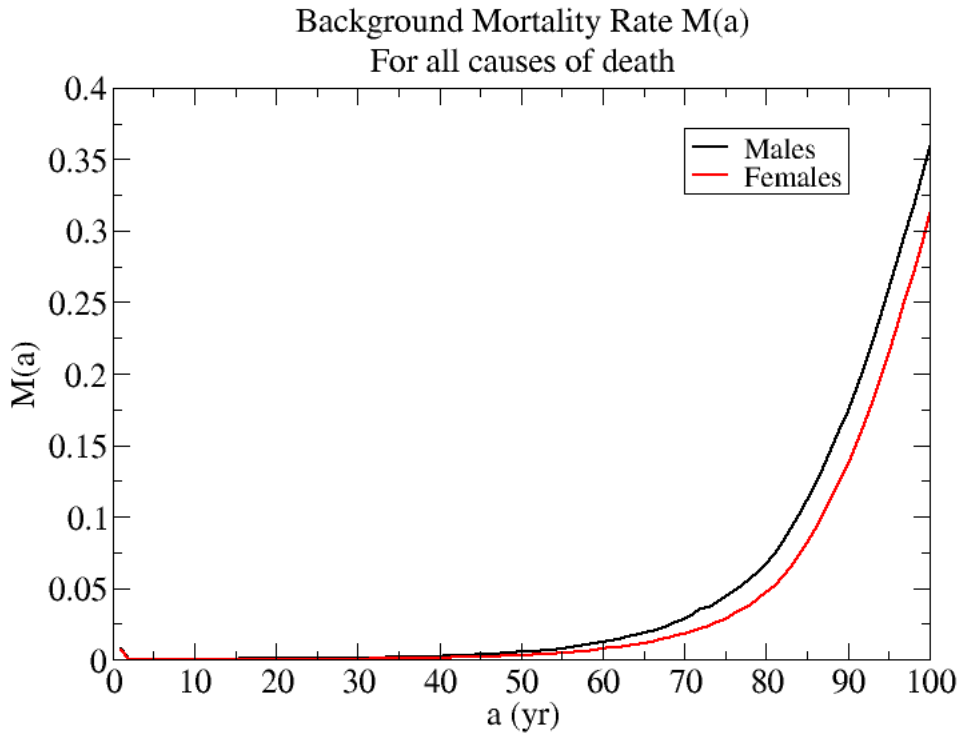

Figure 23: The background mortality rate for all causes of death for males and females.

a lifetime is cumulative, as it depends on prior risk of death. The background probability of survival and death for males is shown in Figure 24. Note that the probability of survival approaches zero at 100 years of age, but it does not quite reach zero. This is consistent with the NVSR [15]. The usual convention is to set the probability of survival to zero for all ages greater than 100 years, instead of using equation (8) to calculate the probability of survival for those years.

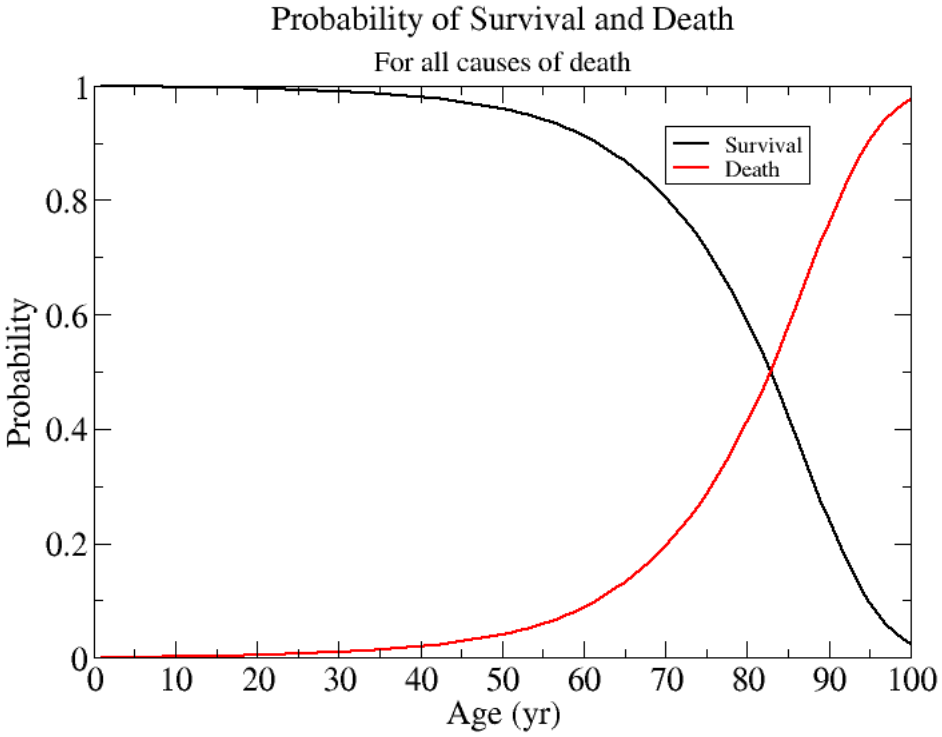

Figure 24: The probability of survival and death for all causes of death for males.

Cancer mortality rates are taken from Surveillance Epidemiology and End Results (SEER) [16], which lists the mortality data differently than the NVSR. In the SEER report, the mortality rate times 100,000 is listed as "mortality rate", but the true cancer mortality rate is obtained by dividing by 100,000, as is seen in Table 7. Also note that SEER gives the cancer mortality rate for all causes of cancer. The solid cancer mortality rate was obtained by subtracting the leukemia mortality rate from the total cancer mortality rate. Finally, note that the data in Tables 7 and 8 are given in abridged form. For example, years 1-4 are grouped together for one mortality rate. It is assumed that the mortality rate is constant for all of the years in a given group.

Table 7: A portion of the abridged solid cancer mortality table for males.

Age at Death (yr)	Cancer Mortality Rate $m_c^S(a) \times 100000$	Cancer Mortality Rate $m_c^S(a)$
< 1	1.5	0.000015
1-4	2.0	0.000020
5-9	1.9	0.000019
10-14	1.7	0.000017
15-19	2.9	0.000029

Table 8: A portion of the abridged leukemia mortality table for males.

Age at Death (yr)	Cancer Mortality Rate $m_c^L(a) \times 100000$	Cancer Mortality Rate $m_c^L(a)$
< 1	0.7	0.000007
1-4	0.9	0.000009
5-9	0.8	0.000008
10-14	1.1	0.000011
15-19	1.3	0.000013

The lifetime risk of dying from solid cancer and leukemia is given in Figure 25. The solid cancer mortality rate was modeled by Kellerer et al. [4] in which the average mortality rate for a span of several years was used. This model will be slightly different from the mortality data used in the present work. Nonetheless, the Kellerer et al. [4] model of the solid cancer mortality rate may be used to confirm the mortality data. In addition,

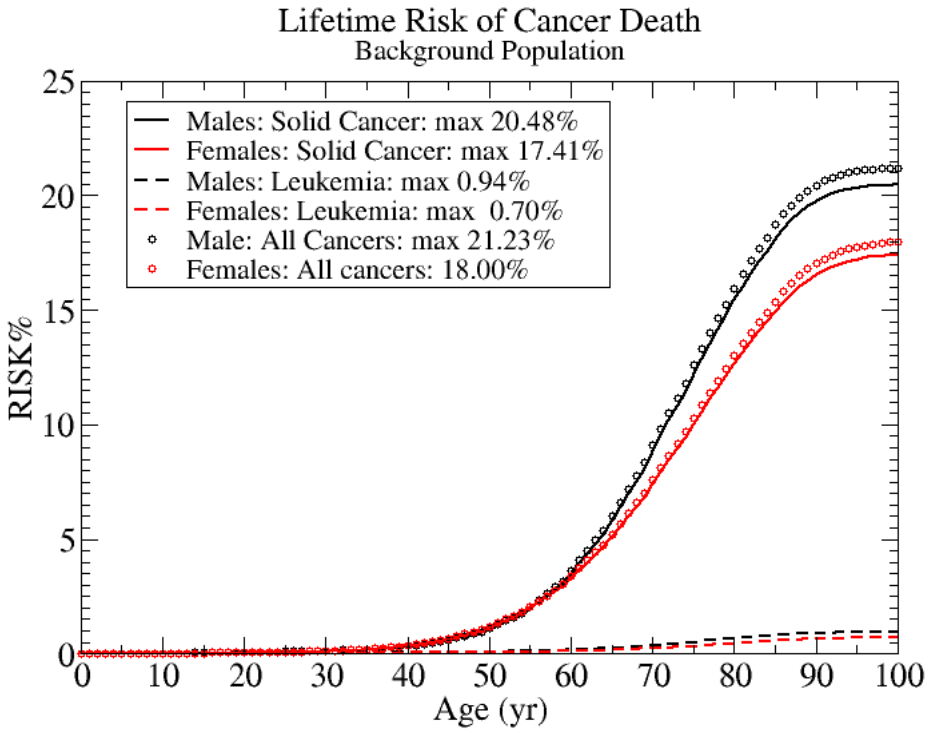

Figure 25: The lifetime risk of dying from solid cancer and leukemia.

the authors of the present work propose a new parametrization for the leukemia mortality rate. The cancer mortality rates are modeled by [4]

$$m_c(a) = k\left(\frac{a}{60}\right)^r \exp\left[-0.06\left(\frac{a}{60}\right)^r\right] + c, \tag{61}$$

where a is the age, and sex dependent parameters are given in the Table 9. In Figure 26, the solid cancer mortality rate and the Kellerer et al. [4] model for males and females have been plotted. In Figure 27, a similar fit has been used for leukemia mortality data.

Table 9: Sex dependent parameters for cancer mortality rates for equation (61). This model may be used in lieu of actual mortality data for testing purposes. The solid cancer parameters are given in reference [4].

Solid		k	r	c
	males	0.0045	6.0	0.0004
	females	0.0030	5.0	0.0004
Leukemia		k	r	c
	males	0.0001981	6.081	0.0
	females	0.0001108	5.968	0.0

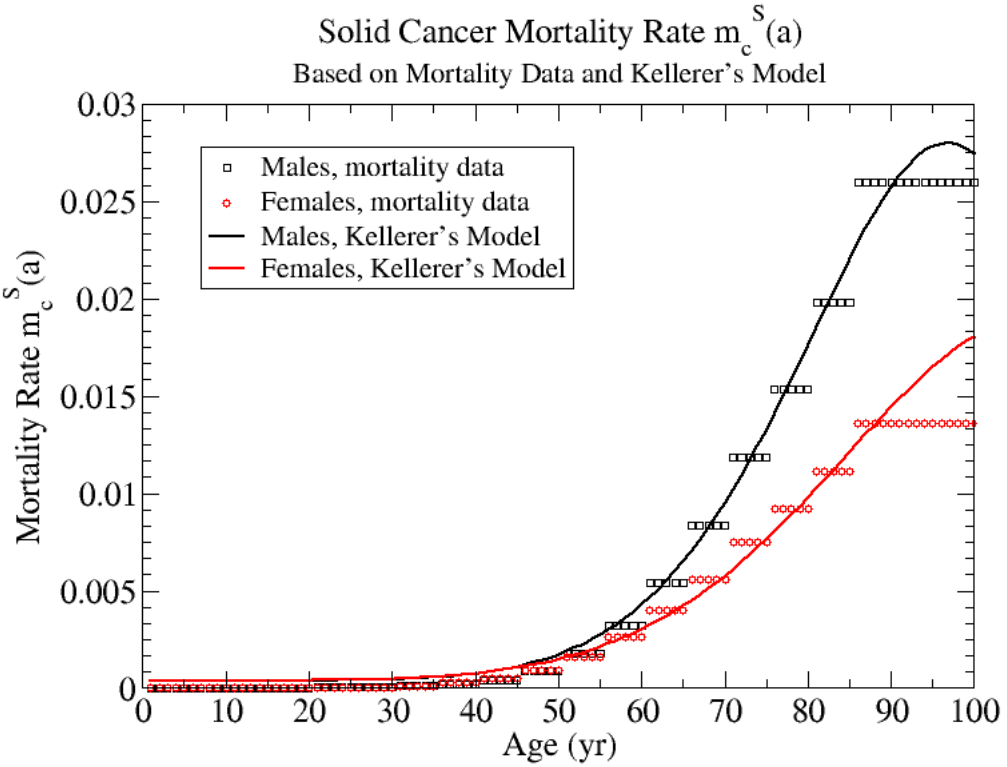

Figure 26: The solid cancer mortality data and the Kellerer et al. [4] model for males and females.

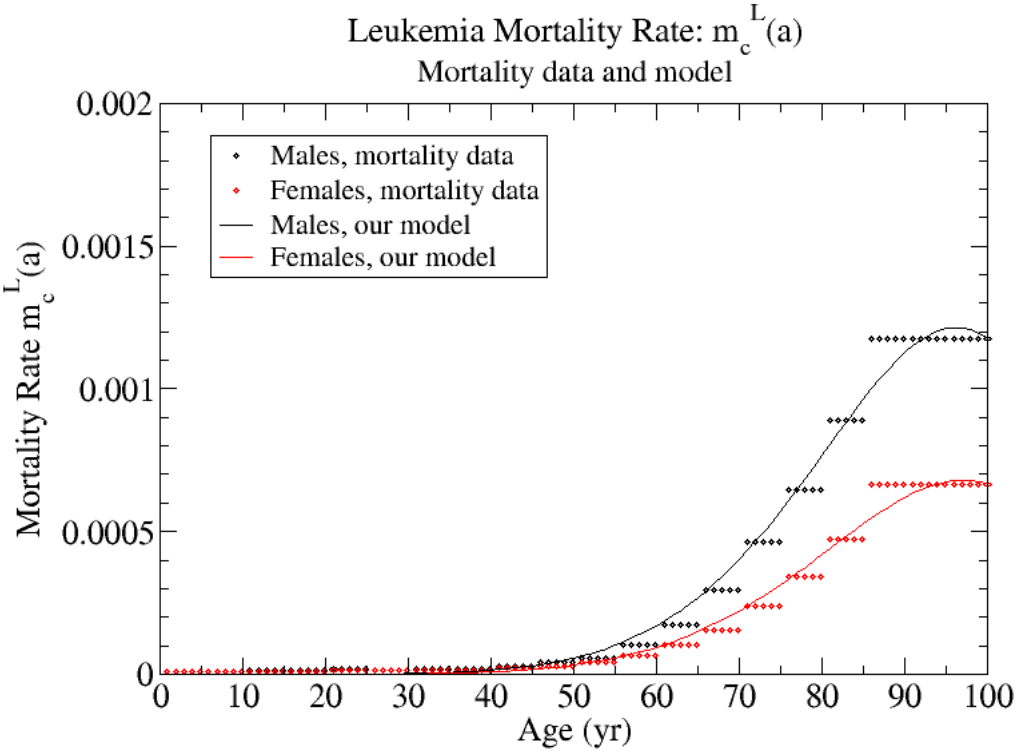

Figure 27: The leukemia mortality data for males and females.

B Monte Carlo Sampling

The acceptance-rejection algorithm for sampling PDFs is discussed in this section and follows the description given in reference [33].

A deviate (or quantile) is a randomly sampled variable. Suppose there exists a function $\rho(x)$, as in Figure 28. Randomly sampled x-values of the $\rho(x)$ function are known as x-deviates. Likewise, random samplings of y-axis are known as y-deviates. The aim of sampling is to find a unique value of the random deviate x for a corresponding value of $\rho(x)$. The idea is to randomly sample a y-deviate and to find the corresponding x-deviate. A distribution of x-deviates will be accumulated after many Monte Carlo trials are binned. Unfortunately, for distributions such as $\rho(x)$ in Figure 28, any randomly sampled y-deviate is associated with two x-deviates. To avoid this problem, the PDF $\rho(x)$ is covered with a Lorentzian function $f(x)$, which is everywhere larger than $\rho(x)$. The Lorentzian distribution function is given by

$$f(x) = \frac{c_0}{1 + (x - x_0)^2/a_0^2}, \tag{62}$$

where c_0, x_0, and a_0 are chosen such that $f(x)$ is everywhere greater than $\rho(x)$. The Lorentzian function is integrated, which results in

$$F(x) = \int f(x)dx = a_0 c_0 \arctan\left(\frac{x - x_0}{a_0}\right). \tag{63}$$

$F(x)$ is a monotonically increasing function and is ideal for sampling, because a randomly sampled y-deviate will correspond to exactly one x-deviate. The minimum $A_{\min}$ and maximum $A_{\max}$ of the integrated Lorentzian in equation (63) are needed for sampling purposes; $A_{\min} = F(x_{\min})$ and $A_{\max} = F(x_{\max})$, where $x_{\min}$ and $x_{\max}$ are the minimum and maximum x-deviates from $\rho(x)$. Samples can be obtained directly from the integrated Lorentzian $F(x)$, which was chosen because it can be easily inverted to produce a unique x-deviate:

$$x = x_0 + a_0 \tan\left(\frac{F(x)}{a_0 c_0}\right). \tag{64}$$

Next, a random deviate y_1 is sampled from $F(x)$ such that $y_1 \epsilon [A_{\min}, A_{\max}]$. The integrated function F(x) is inverted and the corresponding value x_1 is calculated. At this point, x_1 must be accepted or rejected as a deviate. In order to decide this, a new random number r is generated between 0 and $f(x_1)$. If $r \leq p(x_1)$, then x_1 is retained as a deviate, otherwise another random sample is taken from $F(x)$, and the entire process is repeated.

As an example of the acceptance-rejection method, consider the following probability

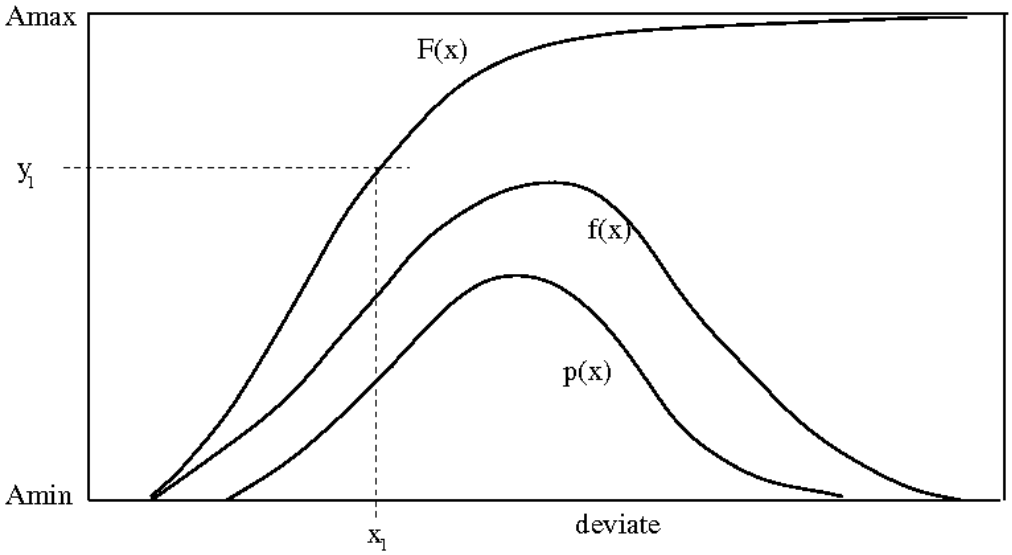

Figure 28: A Lorentzian function $f(x)$ is integrated resulting in $F(x)$, an invertable function. The minimum and maximum areas (Amin and Amax) are calculated. A random value y_1 is generated between Amin and Amax and the corresponding x_1 value is obtained by inverting $F(x_1)$, since $y_1 = F(x_1)$. Next, a random number (r) is generated between 0 and $f(x_1)$. If $r \leq p(x_1)$ then x_1 is retained as the random deviate.

distribution function:

$$\rho(x) = \begin{cases} x - 1 & \text{for } 1 \leq x < 2 \\ 3 - x & \text{for } 2 \leq x \leq 3 \\ 0 & \text{elsewhere.} \end{cases} \tag{65}$$

$\rho(x)$ is covered with a truncated Lorentzian function $f(x)$ with parameters $c_0 = 2$, $x_0 = 2$, $a_0 = 1$, as in Figure 29. $f(x)$ is integrated to obtain an invertible function $F(x)$, as shown

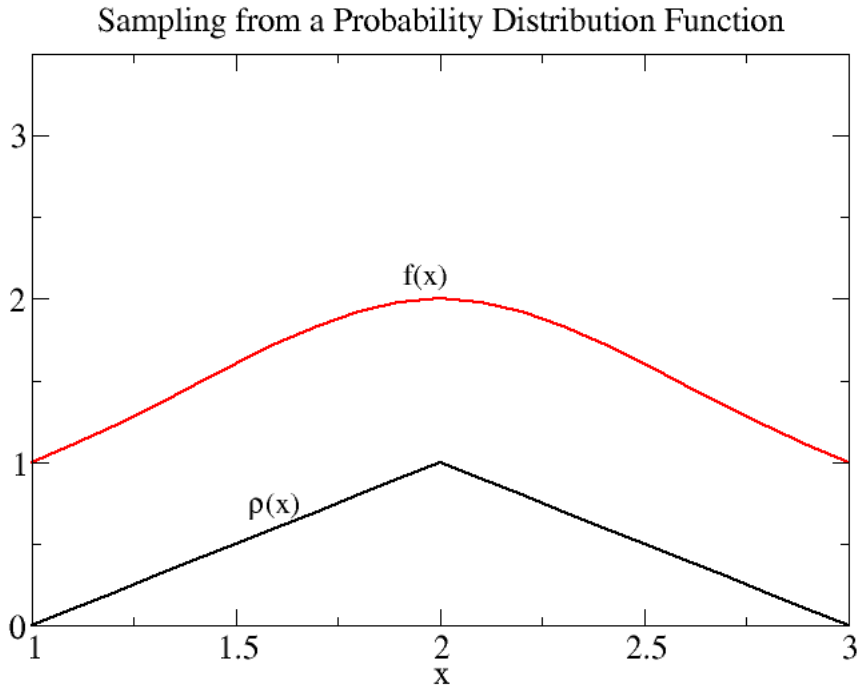

Figure 29: The Probability Distribution Function $\rho(x)$ is covered with a truncated Lorentzian $f(x)$.

in Figure 30. A random number y_1 is generated between $F(1) = -1.57$ and $F(3) = 1.57$. In this example, the randomly sampled y-deviate is $y_1 = 0.49$ and the corresponding x-deviate is $x_1 = 2.25$, which is found from equation (64). Next, as seen in Figure 31, a random number r is generated between 0 and $\rho(x_1) = 0.75$. Two cases must be considered. If the random number generated is less than $\rho(x_1) = 0.75$, such as $r = r_1 = 0.4$, then $x_1 = 2.25$ is accepted as the x-deviate. If, instead, a random number r is generated that is larger than $\rho(x_1) = 0.75$, such as $(r = r_2 = 1.4)$, then $x_1 = 2.25$ is rejected as the

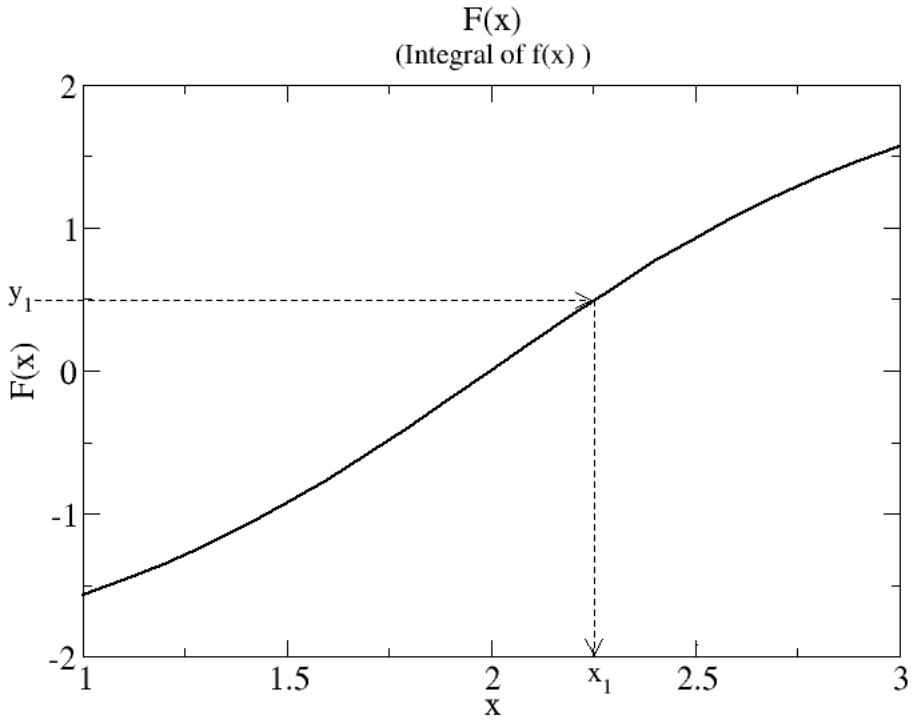

Figure 30: The Lorentzian function is integrated resulting in F(x). A random deviate y_1 is selected and is inverted to find the corresponding x_1 deviate.

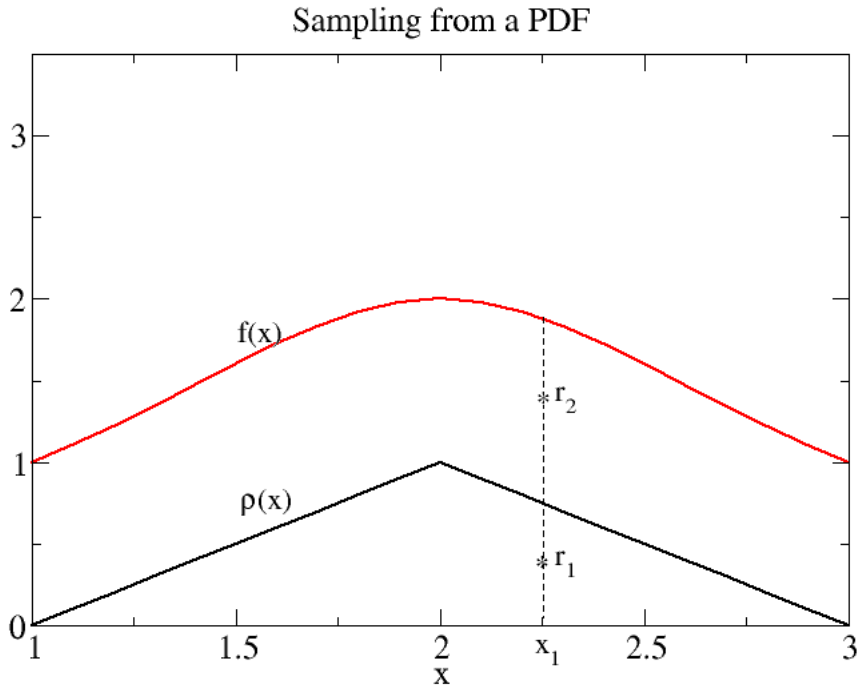

Figure 31: A random number r is generated between 0 and $f(x_1)$. If the random number $r = r_1$ is less than or equal to $\rho(x_1)$, then x_1 is retained as a deviate. If the random number $r = r_2$ is greater than $\rho(x_1)$, then x_1 is rejected as a deviate.

x-deviate. If the x-deviate is rejected, then the whole process begins again with a newly selected random deviate y_1 as in Figure 29.

The Lorentzian parameters and the limits of integration for all of the samplings are listed in Table 10. For numerical sampling efficiency, the parameters of the covering function are adjusted in such a way that there is minimum difference between the covering function and the PDF. It is assumed that the Gaussian distributions described for the fluence uncertainties are zero for all negative valued quantiles. This is a reasonable approximation for the given standard deviations. However, care should be taken in the future if the standard deviations of the Gaussian distributions are increased. A negative-valued quantile could result in a negative effective dose, which is an unphysical result.

Table 10: Lorentzian Parameters used for Monte Carlo Sampling. The min and max values indicate the minimum and maximum range of the sampling. Negative valued quantiles are excluded from the physics uncertainty.

	c_0	a_0	x_0	min	max
Physics Uncertainty					
LET $<$ 30 keV/μm	5.5	0.13	1.0	0	∞
30 $<$ LET $<$ 300 keV/μm	3.1	0.18	1.0	0	∞
LET $\geq$ 300 keV/μm	2.3	0.24	1.0	0	∞
Low LET Uncertainty					
Dosimetry	3.7	0.15	0.84	$-\infty$	∞
Statistical	2.7	0.2	1.0	$-\infty$	∞
Bias	8.0	0.07	1.1	$-\infty$	∞
Transfer	1.6	0.4	0.94	0	∞
DDREF	0.55	1.2	2.1	1	5
Quality Factor Uncertainty					
L_0	1.2	6.0	7.5	1	15
L_m	1.2	100	115	50	250
p	1.2	1.0	0.7	0	2
Q_m	0.025	30	17	0	∞

C Median and 95% Confidence Interval

Samples of the the effective dose and the REID% were accumulated with 20,000 Monte Carlo trials, and the results were binned in histograms, each of which are divided into 2000 bins. The median and 95% CI were also calculated. The median for a given distribution is the point that divides the area into two equal (50%) halves, as in Figure 32. The next task is to estimate the 95% confidence interval. The point along the x-axis that corresponds to 2.5% of the total area is identified as the lower bound of the confidence interval. The upper bound of the CI is found the same way at 97.5% of the total area. The total area that has been excluded for this analysis is 5.0%. The 95% CI is bounded between the upper and lower limits obtained by examining the areas, as in Figure 32. Integration was performed between consecutive points utilizing 5 point Gaussian quadrature, and linear interpolation was used between consecutive points in the histogram data file. Due to the many fluctuations in the histogram data, future algorithms should first smooth the data before integration.

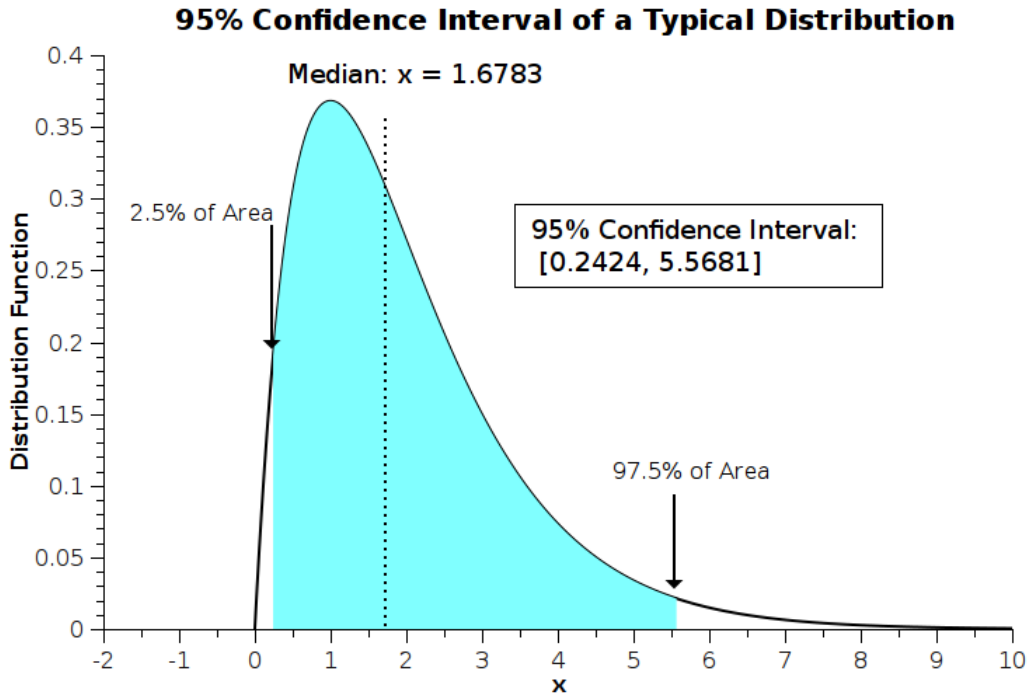

Figure 32: An example of the median and 95% confidence interval.

References

[1] E. R. Benton and E. V. Benton. Space radiation dosimetry in low-Earth orbit and beyond. *Nucl. Instr. Meth. Phys. Res. B*, 184:255, 2001.

[2] NASA Technical Standard 3001. NASA space flight human system standard volume 1: crew health, Washington, DC, 2007.

[3] F. A. Cucinotta, M. Y. Kim, and L. Ren. Evaluating shielding effectiveness for reducing space radiation cancer risks. *Radiat. Meas.*, 41:1173, 2006.

[4] A. M. Kellerer, E. A. Nekolla, and L. Walsh. On the conversion of solid cancer excess relative risk into lifetime attributable risk. *Radiat. Environ. Biophys.*, 40:249, 2001.

[5] M. Vaeth and D. A. Pierce. Calculating excess lifetime risk in relative risk models. *Environ. Health Perspect.*, 87:83, 1990.

[6] D. Thomas, S. Darby, F. Fagnani, P. Hubert, M. Vaeth, and K. Weiss. Definition and estimation of lifetime detriment from radiation exposures: Principals and methods. *Health Phys.*, 63:259, 1992.

[7] U. Schneider and L. Walsh. Cancer risk above 1 Gy and the impact for space radiation protection. *Adv. Space Res.*, 44:202, 2009.

[8] NCRP. National Council of Radiation Protection and Measurements, NCRP Report No. 126. Uncertainties in fatal cancer risk estimates used in radiation protection, Bethesda, MD, 1997.

[9] D. A. Pierce, Y. Shimizu, D. L. Preston, M. Vaeth, and K. Mabuchi. Studies of the mortality of atomic bomb survivors. Report 12, Part 1. Cancer: 1950-1990. *Radiat. Res.*, 146:1, 1996.

[10] D. L. Preston, D. A. Pierce, Y. Shimizu, H. M. Cullings, S. Fujita, S. Funamoto, and K. Kodama. Effect of recent changes in atomic bomb survivor dosimetry on cancer mortality risk estimates. *Radiat. Res.*, 162:377, 2004.

[11] D. L. Preston, Y. Shimizu, D. A. Pierce, A. Suyama, and K. Mabuchi. Studies of mortality of atomic bomb survivors. Report 13: solid cancer and noncancer disease mortality: 1950-1997. *Radiat. Res.*, 160:381, 2003.

[12] ICRP. 1990 Recommendations of the International Commission on Radiological Protection, ICRP publication 60. *Ann. ICRP*, 20(1-3), 1991.

[13] M. Durante and F. A. Cucinotta. Physical basis of radiation protection in space travel. *Rev. Mod. Phys.*, 83:1245, 2011.

[14] T. C. Slaba, S. R. Blattnig, F. F. Badavi, N. N. Stoffle, R. D. Rutledge, K. T. Lee, E. N. Zapp, T. P. Dachev, and B. T. Tomov. Statistical validation of HZETRN as a function of vertical cutoff rigidity using ISS measurements. *Adv. Space Res.*, 47:600, 2011.

[15] E. Arias. United States life table, 2000. *National Vital Statistics Reports*, 51:1, 2002.

[16] S. F. Altekruse et al. SEER cancer statistics review, 1975-2007, National Cancer Institute, Bethesda, MD, `http://seer.cancer.gov/csr/1975_2007/`, 2010.

[17] B. M. Bunger, J. R. Cook, and M. K. Barrick. Life table methodology for evaluating radiation risk: an application based on occupational exposures. *Health Phys.*, 40:439, 1981.

[18] National Research Council. Managing space radiation: Risk in the new era of space exploration. The National Academies Press, Washington, DC, 2008.

[19] C. J. Joachain. *Quantum collision theory.* American Elsevier, New York, NY, 1983.

[20] J. W. Wilson, L. W. Townsend, W. Schimmerling, G. S. Khandelwal, F. Khan, J. E. Nealy, F. A. Cucinotta, L. C. Simonsen, J. L. Shinn, and J. W. Norbury. Transport methods and interactions for space radiations. NASA Reference Publication 1257, 1991.

[21] T. C. Slaba, S. R. Blattnig, and F. F. Badavi. Faster and more accurate transport procedures for HZETRN. *J. Comp. Phys.*, 229:9397, 2010.

[22] T. C. Slaba, S. R. Blattnig, M. S. Clowdsley, S. A. Walker, and F. F. Badavi. An improved neutron transport algorithm for HZETRN. *Adv. Space Res.*, 46:800, 2010.

[23] N. Tsoulfanidis. *Measurement and detection of radiation.* Taylor & Francis, Washington, DC, 1995.

[24] NCRP. National Council of Radiation Protection and Measurements, NCRP Report No. 153. Information needed to make radiation protection recommendations for space missions beyond low-Earth orbit, Bethesda, MD, 2006.

[25] BEIR-VII Phase 2. Health risks from exposure to low levels of ionizing radiation. The National Academic Press, Washington, DC, 2006.

[26] E. J. Hall and A. J. Giaccia. *Radiobiology for the radiologist.* Lippincott Williams & Wilkins, Philadelphia, PA, 1995.

[27] J. H. King. Solar proton fluences for 1977-1983 space missions. *J. Spacecraft Rockets*, 11:401, 1974.

[28] P. M. O'Neill. Badwhar-O'Neill galactic cosmic ray model update based on advanced composition explorer (ACE) energy spectra from 1977 to present. *Adv. Space Res.*, 37:1727, 2006.

[29] W. R. Yucker and S. L. Huston. The computerized anatomical female. MDC-6107, McDonnell Douglas Company, 1990.

[30] W. R. Yucker and R. J. Reck. The computerized anatomical female body self-shielding distributions. MDC-92H0749, McDonnell Douglas Company, 1992.

[31] H. S. Shryock. *The methods and materials of demography.* U.S. Government Printing Office, Washington, DC, 1975.

[32] C. L. Chiang. *Introduction to stochastic processes in biostatistics.* John Wiley & Sons, New York, NY, 1968.

[33] W. H. Press, S. A. Teukolsky, W. T. Vetterling, and B. P. Flannery. *Numerical recipes in FORTRAN.* Cambridge University Press, New York, NY, 1992.

REPORT DOCUMENTATION PAGE

Form Approved
OMB No. 0704-0188

1. REPORT DATE *(DD-MM-YYYY)*	2. REPORT TYPE	3. DATES COVERED *(From - To)*
01-02-2013	Technical Publication	

4. TITLE AND SUBTITLE

Correlated Uncertainties in Radiation Shielding Effectiveness

5a. CONTRACT NUMBER

5b. GRANT NUMBER

5c. PROGRAM ELEMENT NUMBER

6. AUTHOR(S)

Werneth, Charles M.; Maung, Khin Maung; Blattnig, Steve R.; Clowdsley, Martha S.; Townsend, Lawrence R.

5d. PROJECT NUMBER

5e. TASK NUMBER

5f. WORK UNIT NUMBER

651549.02.07.01

7. PERFORMING ORGANIZATION NAME(S) AND ADDRESS(ES)

NASA Langley Research Center
Hampton, VA 23681-2199

8. PERFORMING ORGANIZATION REPORT NUMBER

L-20224

9. SPONSORING/MONITORING AGENCY NAME(S) AND ADDRESS(ES)

National Aeronautics and Space Administration
Washington, DC 20546-0001

10. SPONSOR/MONITOR'S ACRONYM(S)

NASA

11. SPONSOR/MONITOR'S REPORT NUMBER(S)

NASA/TP-2013-217965

12. DISTRIBUTION/AVAILABILITY STATEMENT

Unclassified - Unlimited
Subject Category 93
Availability: NASA CASI (443) 757-5802

13. SUPPLEMENTARY NOTES

14. ABSTRACT

The space radiation environment is composed of energetic particles which can deliver harmful doses of radiation that may lead to acute radiation sickness, cancer, and even death for insufficiently shielded crew members. Spacecraft shielding must provide structural integrity and minimize the risk associated with radiation exposure. The risk of radiation exposure induced death (REID) is a measure of the risk of dying from cancer induced by radiation exposure. Uncertainties in the risk projection model, quality factor, and spectral fluence are folded into the calculation of the REID by sampling from probability distribution functions. Consequently, determining optimal shielding materials that reduce the REID in a statistically significant manner has been found to be difficult. In this work, the difference of the REID distributions for different materials is used to study the effect of composition on shielding effectiveness. The use of correlated uncertainties allows for the determination of statistically significant differences between materials despite the large uncertainties in the quality factor. This is in contrast to previous methods where uncertainties have been generally treated as uncorrelated. It is concluded that the use of correlated quality factor uncertainties greatly reduces the uncertainty in the assessment of shielding effectiveness for mitigation of radiation exposure.

15. SUBJECT TERMS

Effective Dose; Quality Factor; Radiation Exposure

16. SECURITY CLASSIFICATION OF:			17. LIMITATION OF ABSTRACT	18. NUMBER OF PAGES	19a. NAME OF RESPONSIBLE PERSON
a. REPORT	b. ABSTRACT	c. THIS PAGE			STI Help Desk (email: help@sti.nasa.gov)
					19b. TELEPHONE NUMBER *(Include area code)*
U	U	U	UU	70	(443) 757-5802